DESY 13-183
DO-TH 13/26
LPN 13-068
SFB/CPP-13-71
October 2013

The ABM parton distributions tuned to LHC data

S. Alekhin[a,b,1], J. Blümlein[a,2], and S. Moch[a,c,3]

[a] *Deutsches Elektronensynchrotron DESY*
Platanenallee 6, D–15738 Zeuthen, Germany

[b] *Institute for High Energy Physics*
142281 Protvino, Moscow region, Russia

[c] *II. Institut für Theoretische Physik, Universität Hamburg*
Luruper Chaussee 149, D–22761 Hamburg, Germany

Abstract

We present a global fit of parton distributions at next-to-next-to-leading order (NNLO) in QCD. The fit is based on the world data for deep-inelastic scattering, fixed-target data for the Drell-Yan process and includes, for the first time, data from the Large Hadron Collider (LHC) for the Drell-Yan process and the hadro-production of top-quark pairs. The analysis applies the fixed-flavor number scheme for $n_f = 3,4,5$, uses the $\overline{\rm MS}$ scheme for the strong coupling α_s and the heavy-quark masses and keeps full account of the correlations among all non-perturbative parameters. At NNLO this returns the values of $\alpha_s(M_Z) = 0.1132 \pm 0.0011$ and $m_t(\text{pole}) = 171.2 \pm 2.4$ GeV for the top-quark pole mass. The fit results are used to compute benchmark cross sections for Higgs production at the LHC to NNLO accuracy. We compare our results to those obtained by other groups and show that differences can be linked to different theoretical descriptions of the underlying physical processes.

[1] **e-mail**: sergey.alekhin@ihep.ru
[2] **e-mail**: johannes.bluemlein@desy.de
[3] **e-mail**: sven-olaf.moch@desy.de

1 Introduction

Our knowledge of the proton structure builds on the accumulated world data from the deep-inelastic scattering (DIS) experiments, which cover a broad kinematic range in terms of the scaling variable x and the momentum Q^2 transferred to the proton [1]. These data have been gathered in a variety of different scattering experiments, either on fixed targets or through colliding beams, and in the past two decades, especially the HERA electron-proton collider has contributed significantly with very accurate measurements spanning a wide range in x and Q^2. Thus, DIS world data form the backbone for the determination of the parton distribution functions (PDFs) in the QCD improved parton model.

Modern PDFs, however, are expected to provide an accurate description of the parton content of the proton not only in a kinematic region for x and Q^2 as wide as possible, but to deliver also information on the flavor composition of the proton as well as on other non-perturbative parameters associated to the observables under consideration, such as the strong coupling constant α_s or the masses of the heavy quarks charm, bottom and top. In the theoretical predictions the values for these quantities are often correlated with the PDFs and, therefore, have to be determined simultaneously in a fit.

A comprehensive picture of a composite object such as the proton does not emerge without the need for additional assumptions by relying, e.g., on DIS data from the HERA collider alone. Therefore, global PDF fits have to include larger sets of precision data for different processes, which have to be compatible, though. The release of the new data for so-called standard candle processes, i.e., precisely measured and theoretically well-understood Standard Model (SM) scattering reactions, initiates three steps in the analysis:

i) check of compatibility of the new data set with the available world data

ii) study of potential constraints due to the addition of the new data set to the fit

iii) perform a high precision determination of the non-perturbative parameters: PDFs, $\alpha_s(M_Z)$ and heavy-quark masses.

Of course, at every step QCD precision analyses have to provide a detailed account of the systematic errors and have to incorporate all known theoretical corrections. At the Large Hadron Collider (LHC) PDFs are an indispensable ingredient in almost every experimental analysis and the publication of data for $W^{\pm}$- or Z-boson, top-quark pair or jet-production from the runs at $\sqrt{s} = 7$ and 8 TeV center-of-mass (c.m.s.) energy motivates the investigation of potential constraints on SM parameters anew.

Precision data, of course, has to be confronted to high precision theory descriptions. In a hadron collider environment, the reduction of the theoretical uncertainty below $O(10\%)$ cannot be achieved without recourse to predictions at next-to-next-to-leading order (NNLO) in QCD [2, 3] which has thus become the standard paradigm of QCD precision analyses of the proton's parton content [4]. The PDF fits ABKM09 [5] and, subsequently, ABM11 [6] on which the current analysis is building, have been performed precisely in this spirit. At the same time, the NNLO paradigm has motivated continuous improvements in the theory description of processes where only next-to-leading order (NLO) corrections are available, such as the hadro-production of jets.

In the current article, we are, for the first time, tuning the ABM PDFs to the available LHC data for a number of standard candle processes including $W^{\pm}$- and Z-boson production as well as $t\bar{t}$-production. We are demonstrating overall very good consistency of the ABM11 PDFs with the available LHC data. Particular aspects of these findings have been reported previously [7–11].

Subsequently, we perform a global fit to obtain a new ABM12 PDF set and we discuss in detail the obtained results for the PDFs, $\alpha_s(M_Z)$ and the quark masses along with their correlations and the goodness of fit.

The outline of the article is as follows. We recall in Sec. 2 the footing of our fit and present the basic improvements in the theory description and the new data sets included. These encompass the charm-production and high-Q neutral-current HERA data discussed in Sections. 2.1 and 2.2, the $W^{\pm}$- and Z-boson production data from the LHC investigated in Section 2.3 and, likewise, in Sec. 2.4 data for the total cross section of $t\bar{t}$-production. The results for ABM12 PDFs are discussed in Section 3 in a detailed comparison with the ABM11 fit in Sec. 3.1 and with emphasis on the strong coupling constant and the charm quark mass, cf. Section 3.2. Finally, in Section 3.3 we provide cross section predictions of the ABM12 PDFs for a number of standard candle processes and the dominant SM Higgs production channel. Appendix A describes a fast algorithm for dealing with those iterated theoretical computations in the PDF fit, which are very time-consuming.

2 New data included and the theory update

The present analysis is an extension of the earlier ABM11 fit [6] based on the DIS and DY data and performed in the NNLO accuracy. The improvements are related to adding recently published data relevant for the PDF determination:

- semi-inclusive charm DIS production data obtained by combination of the H1 and ZEUS results [12]. This data set provides an improved constraint on the low-x gluon and sea-quark distribution and allows amended validation of the c-quark production mechanism in the DIS.
- the neutral-current DIS inclusive data with the momentum transfer $Q^2 > 1000$ GeV^2 obtained by the HERA experiments [13]. These data allow to check the 3-flavor scheme used in our analysis up to very high momentum transfers and, besides, to improve somewhat the determination of the quark distributions at $x \sim 0.1$.
- the DY data obtained by the LHC experiments [14–17] improve the determination of the quark distribution at $x \sim 0.1$, and in particular provide a constraint on the d-quark distribution, which is not sensitive to the correction on the nuclear effects in deuteron.
- the total top-quark pair-production cross section data from LHC [18–22] and the Tevatron combination [23] provide the possibility for a consistent determination the top-quark mass with full account of the correlations with the gluon PDF and the strong coupling α_s.

The theoretical framework of the analysis is properly improved as compared to the ABM11 fit in accordance with the new data included. In this Section we describe details of these improvements related to each of the processes and the data sets involved, check agreement of the new data with the ABM11 fit, and discuss their impact and the goodness of fit.

2.1 The HERA charm data

The HERA data on the c-quark DIS production [12] are obtained by combination of the earlier H1 and ZEUS results. The combined data span the region of $Q^2 = 2.5 \div 2000$ GeV^2 and $x = 3 \cdot 10^{-5} \div 0.05$. The dominating channel of the c-quark production at this kinematics is the

photon-gluon fusion. Therefore it provides an additional constraint on the small-x gluon distribution. Our theoretical description of the HERA data on charm-production is based on the fixed-flavor-number (FFN) factorization scheme with 3 light quarks in the initial state and the heavy-quarks appearing in the final state. The 3–flavor Wilson coefficients for the heavy-quark electro-production are calculated in NLO [24, 25] and approximate NNLO corrections have been also derived recently [26]. The latter are obtained as a combination of the threshold resummation calculation [27] and the high-energy asymptotics [28] with the available Mellin moments of the massive operator matrix elements (OMEs) [29–32], which provide matching of these two. Two options of the NNLO Wilson coefficient's shape, A and B, given in Ref. [26] encode the remaining uncertainty due to higher Mellin moments than given in [31]. In the present analysis, the NNLO corrections are modeled as a linear combination of the option A and B of Ref. [26] with the interpolation parameter d_N with the values of $d_N = 0, 1$ for the options A and B, respectively. The interpolation parameter is fitted to the data simultaneously with other fit parameters and the shape of the massive NNLO correction preferred by the data is found to be close to option A with the best fit value of $d_N = -0.10 \pm 0.15$. The same approach was also used in our earlier determination of the c-quark mass from the DIS data including the HERA charm-production ones [33] with a similar value of d_N obtained. In our analysis we also employ the running-mass definition for the DIS structure functions [34]. For comparison, the ABM11 fit is based on the massive NNLO corrections stemming from the threshold resummation only [27] and their uncertainty is not considered.

The description of the HERA charm data within the ABM12 framework is quite good with the value of $\chi^2/NDP = 62/52$, where NDP stands for the number of data points. The pulls for this data set also do not demonstrate any statistically significant trend with respect to either x or Q^2, cf. Fig. 2.1. In particular, this gives an argument in favor of using the 3-flavor scheme over the full range of existing DIS data kinematics.

2.2 The high-Q neutral-current HERA data

The HERA data for $Q^2 > 1000$ GeV^2 newly added to our analysis are part of the combined inclusive sample produced using the H1 and ZEUS statistics collected during Run-I of the HERA operation [13]. Due to kinematic constraints of DIS these data are localized at relatively large values of x, where they have limited statistical potential for the PDF constraint as compared to the fixed-target DIS data used in our analysis. For this reason this piece was not used in the ABM11 fit. In the present analysis we fill this gap for the purpose of completeness. At large Q^2 the DIS cross section gets non-negligible contributions due to the Z-exchange, in addition to the photon-exchange term sufficient for the accurate description of the data at $Q^2 \ll M_Z^2$, where M_Z is the Z-boson mass. The Z-boson contribution is taken into account using the formalism [35, 36] with account of the correction to the massless Wilson coefficients up to NNLO [37]. In accordance with [35] the contribution due to the photon-Z interference term dominates over the one for the pure Z-exchange at HERA kinematics [1]. The values of χ^2/NDP obtained in our analysis for the whole inclusive HERA data set and for its neutral-current subset are $694/608$ and $629/540$, respectively. The data demonstrate no statistically significant trend with respect to the fit up to the highest values of Q^2 covered by the data. This is illustrated in Fig. 2.2 with the example of the neutral-current e^+p HERA data sample, which contains the most accurate HERA measurements at large Q^2. For the e^-p sample the picture is similar and the total value of χ^2/NDP obtained for the newly added neutral-current data with $Q^2 > 1000$ GeV^2 is $147/142$. For comparison, with the cuts

[1] The version 1.6 of the `OPENQCDRAD` code used in our analysis to compute the DIS structure functions including the contribution due to the Z-exchange is publicly available online [38].

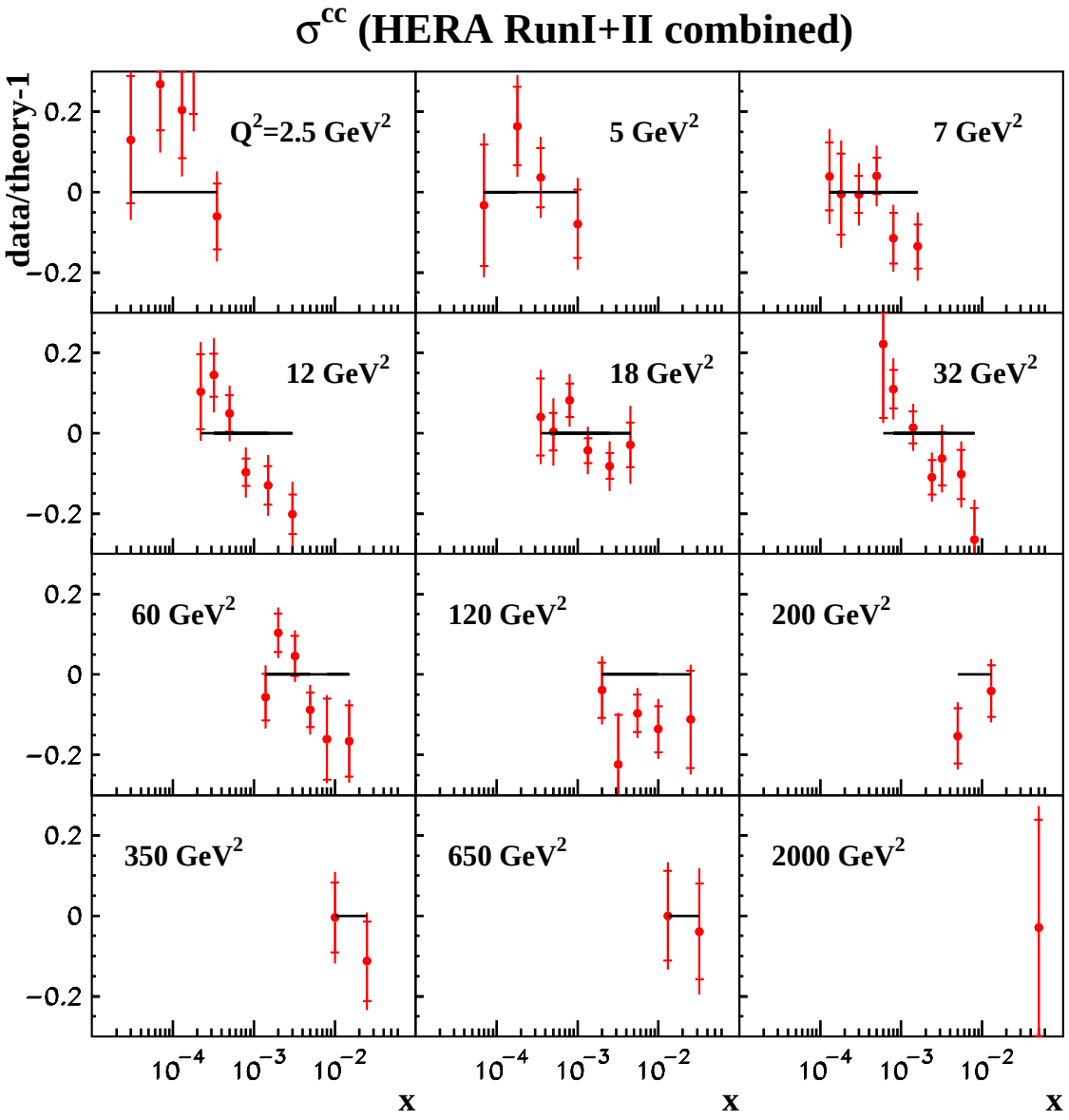

Figure 2.1: The pulls versus Bjorken x for the HERA combined data on the charm production [12] binned in momentum transfer Q^2 with respect to our NNLO fit.

of $Q^2 > 100\ \mathrm{GeV}^2$ and $Q^2 > 10\ \mathrm{GeV}^2$ we get for the same sample the values of $\chi^2/NDP = 311/344$ and 486/469, respectively. In particular this says that the FFN scheme used in our analysis is quite sufficient for the description of the existing HERA data in the whole kinematical range (cf. [39,40] for more details).

2.3 The LHC Drell-Yan data

Data on the Drell-Yan (DY) process provide a valuable constraint on the PDFs extracted from a global PDF fit allowing to disentangle the sea and valence quark distributions. At the LHC these data are now available in the form of the rapidity distributions of charged leptons produced in the decays of the W-bosons and/or charged-lepton pairs from the Z-boson decays [14–17]. Due

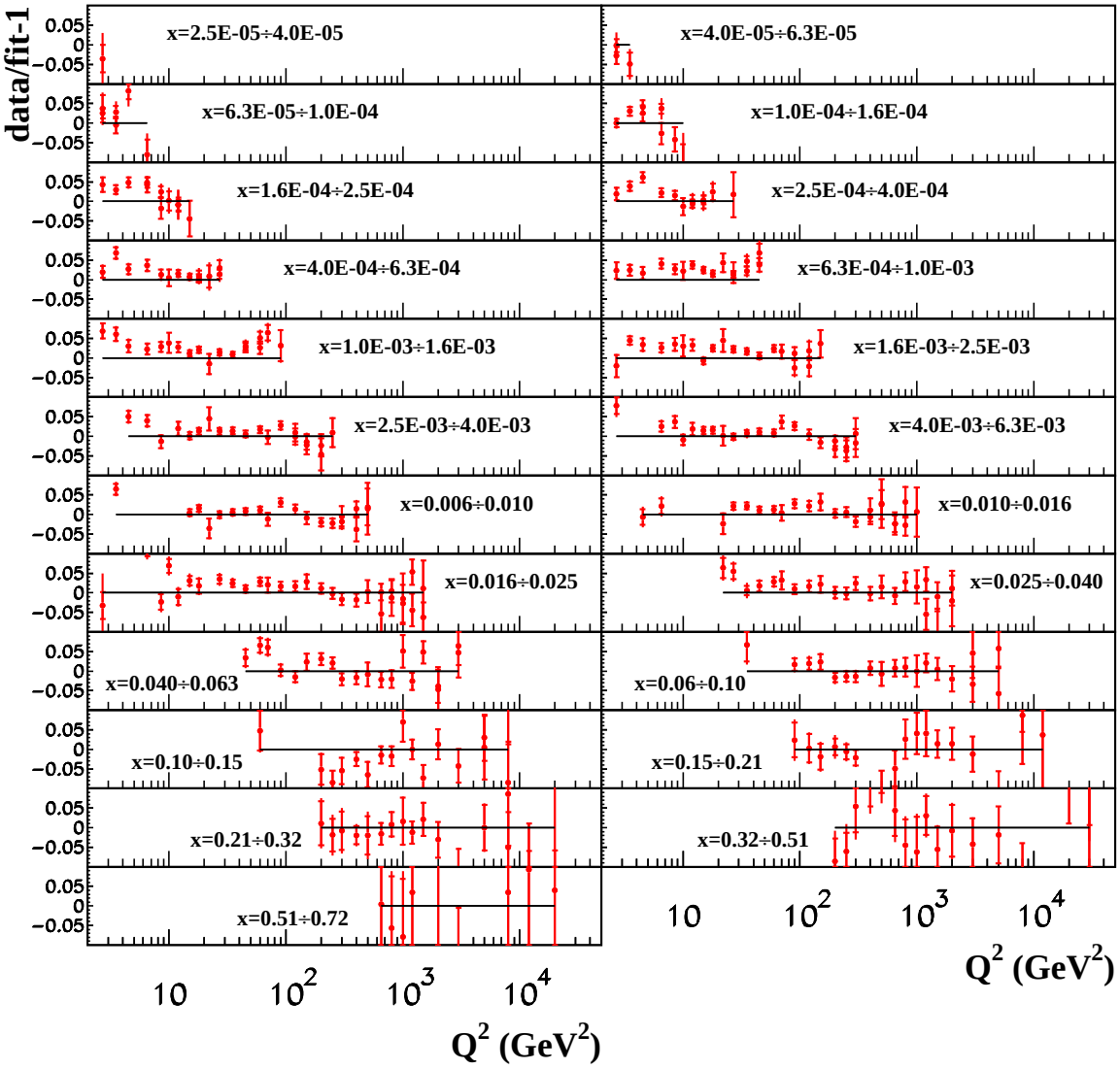

Figure 2.2: The same as in Fig. 2.1 for the pulls of the HERA inclusive combined data [13] binned in Bjorken x versus momentum transfer Q^2.

to limited detector acceptance and the W/Z event selection criteria the LHC data are commonly obtained in a restricted phase space with a cut on the lepton transverse momentum P_T^l imposed. Therefore, taking advantage of these data to constrain the PDFs requires fully exclusive calculations of the Drell-Yan process. These are implemented up to NNLO in two publicly available codes, `DYNNLO` [41] and `FEWZ` [42]. Benchmarking these codes we found good mutual agreement for the LHC kinematics. We note that with the version 1.3 of `DYNNLO` the numerical convergence is achieved faster than for version 3.1 of `FEWZ`, although even in the former case a typical CPU time required for computing rapidity distribution with the accuracy better than 1% is 200 hours for the Intel model P9700/2.80 GHz. However, `FEWZ` (version 3.1) provides a convenient capability to estimate uncertainties in the cross sections due to the PDFs. Therefore we use in our analysis the benefits of both codes combining the central values of `DYNNLO` (version 1.3) and the PDF

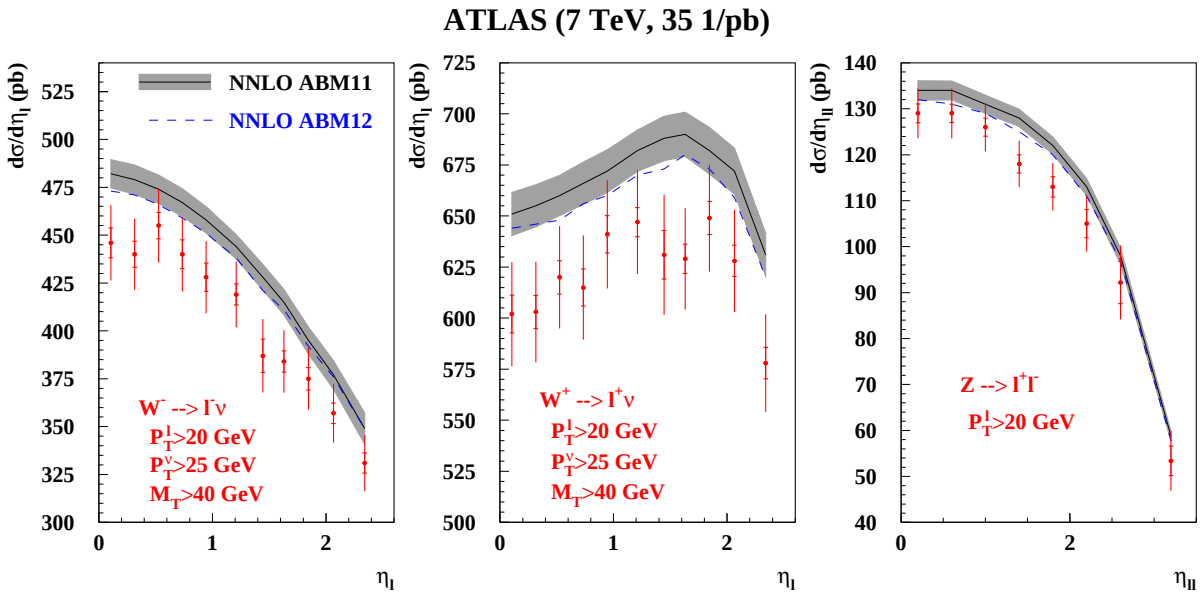

Figure 2.3: The ATLAS data [14] on the rapidity distribution of charged leptons produced in the decays of W^-- and W^+-boson (left and central panel, respectively) and charged lepton pairs from the decays of Z-boson (right panel) in comparison with the NNLO calculations based on the ABM11 PDFs (solid curves) taking into account the uncertainties due to PDFs (grey area). The dashed curves display the ABM12 predictions. The cuts on the lepton transverse momentum P_T^l and the transverse mass M_T imposed to select a particular process signal are given in the corresponding panels.

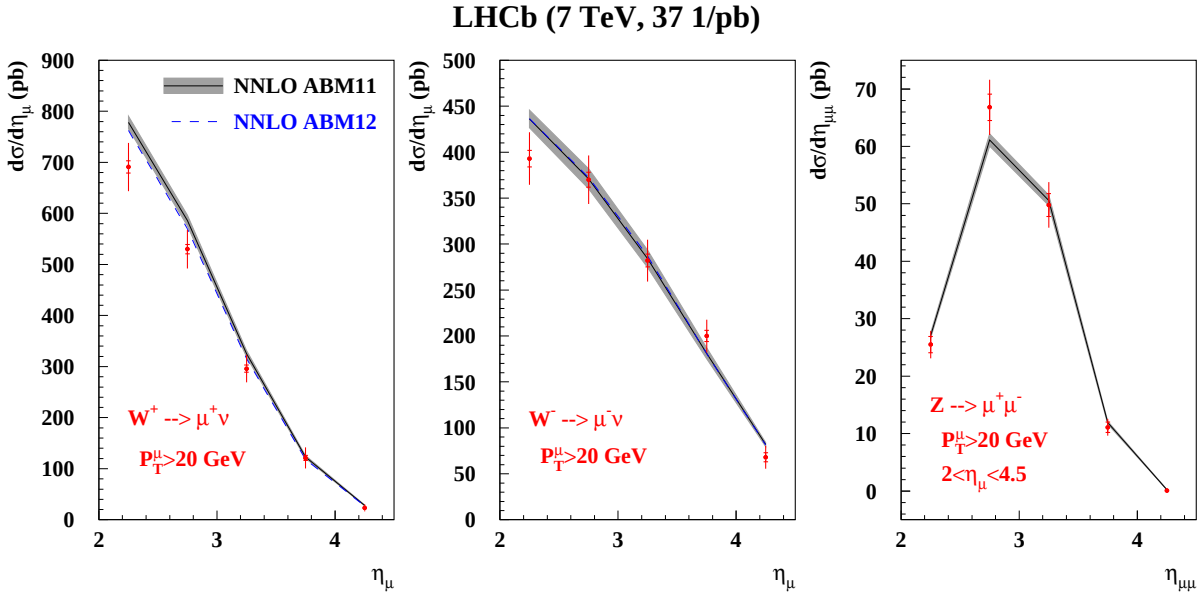

Figure 2.4: The same as in Fig. 2.3 for the charged muons rapidity distributions obtained by LHCb [15].

uncertainties of FEWZ (version 3.1).

The predictions obtained in such a way with the ABM11 PDFs [6] are compared to the LHC DY data [14–17] in Figs. 2.3, 2.4 and 2.5. The predictions systematically overshoot the ATLAS data [14]. However the offset is within the experimental uncertainty, which is dominated by the one of 3.5% due to the luminosity, cf. Fig 2.3. On the other hand, a good agreement is observed

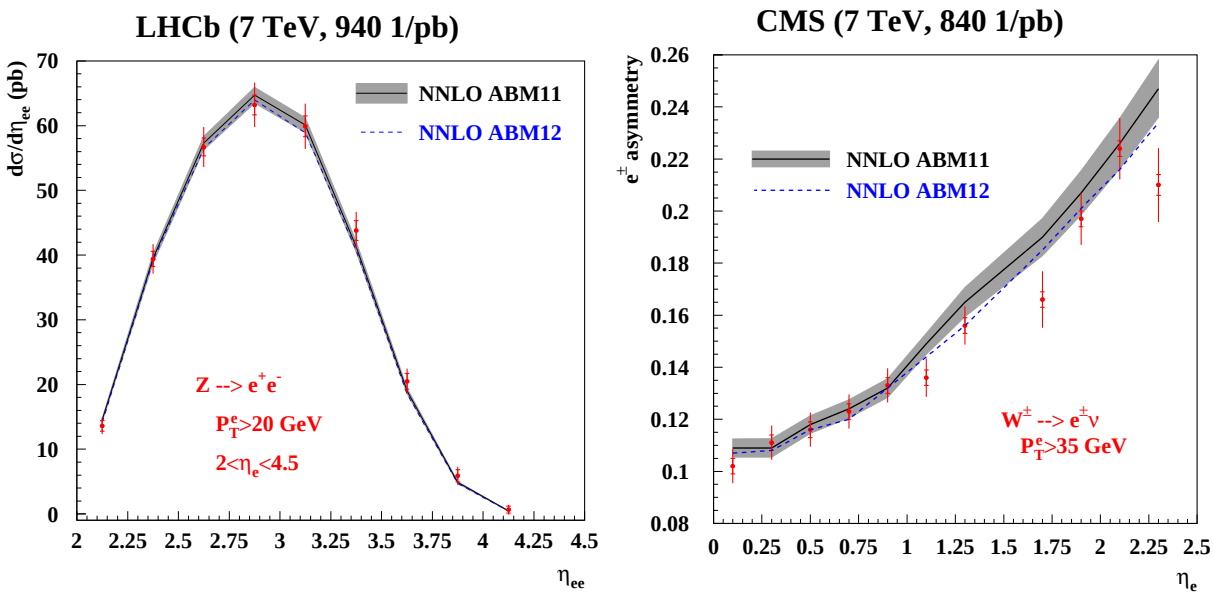

Figure 2.5: The same as in Fig. 2.3 for the LHCb data [17] on the rapidity distribution of the e^+e^- pairs produced in the Z-boson decays (left panel) and the CMS data [16] on the charge asymmetry of electrons produced in the $W^{\pm}$-boson decays (right panel).

for the Z-boson data by LHCb [17] in the region overlapping with the ATLAS kinematics, cf. Fig 2.5. This signals some discrepancy between these two sets of data, which is most likely related to the general experimental normalization. In any case the normalization off-set cancels in the ratio and the ATLAS data on the charged-lepton asymmetry are in a good agreement with our predictions [14]. This is in some contrast to the CMS results where a few data points go lower than the ABM11 predictions, cf. Fig 2.5.

Agreement between the LHC data and the ABM11 predictions is quantified by the following χ^2 functional

$$\chi^2 = \sum_{i,j} (y_i - t_i^{(0)})[C^{-1}]_{ij}(y_j - t_j^{(0)}), \tag{2.1}$$

where y_i and $t_i^{(0)}$ stand for the measurements and predictions, respectively, and C_{ij} is the covariance matrix with the indices i, j running over the points in the data set. The covariance matrix is constructed as follows

$$C_{ij} = C_{ij}^{exp} + \sum_{k=1}^{N_{unc}} \Delta t_i^{(k)} \Delta t_j^{(k)}, \tag{2.2}$$

where the first term contains information about the experimental errors and their correlations and the second term comprises the PDF uncertainties in predictions. The later are quantified as shifts in the predictions due to the variation between the central PDF value and the ones encoding the PDF uncertainties. For ABM11 the latter appear primarily due to the variation of the fitted PDF parameters and, besides, due to the uncertainty in the nuclear correction applied to the deuteron DIS data. Therefore, the total number of PDF uncertainty members is $N_{unc} = N_p + 1$, where $N_p = 27$ is the number of eigenvectors in the space of fitted PDF parameters (cf. the Appendix for more details).

The experimental covariance matrix for the ATLAS data [14] is computed by

$$C_{ij}^{exp} = \delta_{ij}\sigma_i^2 + f_i^{(0)} f_j^{(0)} \sum_{l=1}^{31} s_i^k s_j^k, \tag{2.3}$$

where σ_i are the statistical errors in the data combined in quadrature with the uncorrelated errors. Here s_i^l are the correlated systematic uncertainties representing 31 independent sources including the normalization, and δ_{ij} stands for the Kronecker symbol. In view of the small background for the W- and Z-production signal all systematic errors are considered as multiplicative. Therefore, they are weighted with the theoretical predictions $f_i^{(0)}$. The experimental covariance matrices for the CMS and LHCb data of Refs. [15–17] are employed directly as published in Eq. (2.2) after re-weighting them by the theoretical predictions similarly to Eq. (2.3) with the normalization uncertainty taken into account in the same way as for the ATLAS data.

Experiment	ATLAS [14]	CMS [16]	LHCb [15]	LHCb [17]
Final states	$W^+ \to l^+\nu$ $W^- \to l^-\nu$ $Z \to l^+l^-$	$W^+ \to e^+\nu$ $W^- \to e^-\nu$	$W^+ \to \mu^+\nu$ $W^- \to \mu^-\nu$	$Z \to e^+e^-$
Luminosity (1/pb)	35	840	37	940
NDP	30	11	10	9
χ^2 (ABM11)	35.7(7.7)	10.6(4.7)	13.1(4.5)	11.3(4.2)
χ^2 (ABM12)	35.6	9.3	14.4	13.4

Table 2.1: The value of χ^2 obtained for different samples of the Drell-Yan LHC data with the NNLO ABM11 PDFs in comparison with the one obtained in the ABM12 fit. The figures in parenthesis give one standard deviation of χ^2 equal to $\sqrt{2NDP}$.

The values of χ^2 computed according to Eq. (2.1) for each of the LHC DY data sets obtained with the ABM11 PDFs are given in Tab. 2.1. The description quality is somewhat worse for the ATLAS and LHCb muon data, however, in general the agreement between the data and predictions is still good. The values of χ^2/NDP are comparable to 1 within the statistical fluctuations in χ^2. Therefore, the data can be easily accommodated in the ABM fit. Furthermore, in this case the PDF variation is expected to be within the ABM11 PDF uncertainties. This allows to optimize the computation of the involved NNLO Drell-Yan corrections in the fit by extrapolation of the grid with the pre-calculated predictions for the ABM11 eigenvector basis (cf. App. A for the details on the implementation of this approach). The values of χ^2 obtained for the LHC DY data sets in the ABM12 fit are quoted in Tab. 2.1. In this case the PDF uncertainties are irrelevant since the PDFs have been tuned to the data. Therefore, they are not included into the second term in the covariance matrix Eq. (2.2). Despite the difference in the definition, the ABM12 values of χ^2 for the LHC DY data are in a good agreement with the ABM11 ones giving additional evidence for the compatibility of these data with the ABM11 PDFs.

2.4 The data for $t\bar{t}$ production in the ABM12 fit

At the LHC $t\bar{t}$-pair production proceeds predominantly through initial gluon-gluon scattering. Thus, the total $t\bar{t}$ cross section is sensitive to the gluon distribution at effective x values of $\langle x \rangle \simeq$

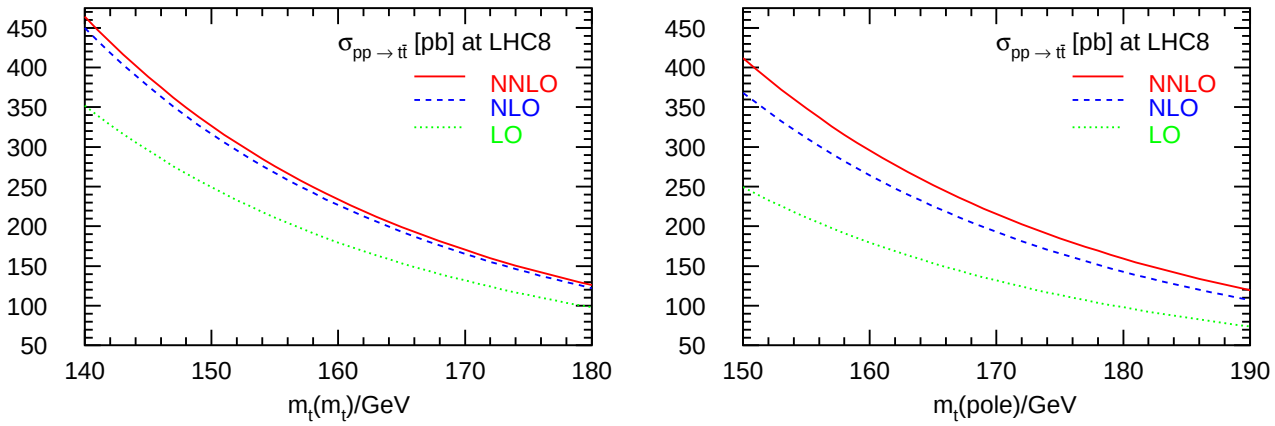

Figure 2.6: The LO, NLO and NNLO QCD predictions for the $t\bar{t}$ total cross section at the LHC ($\sqrt{s}$ = 8 TeV) as a function of the top-quark mass in the $\overline{\rm MS}$ scheme $m_t(m_t)$ at the scale $\mu = m_t(m_t)$ (left) and in the on-shell scheme m_t(pole) at the scale $\mu = m_t$(pole) (right) with the ABM12 PDFs.

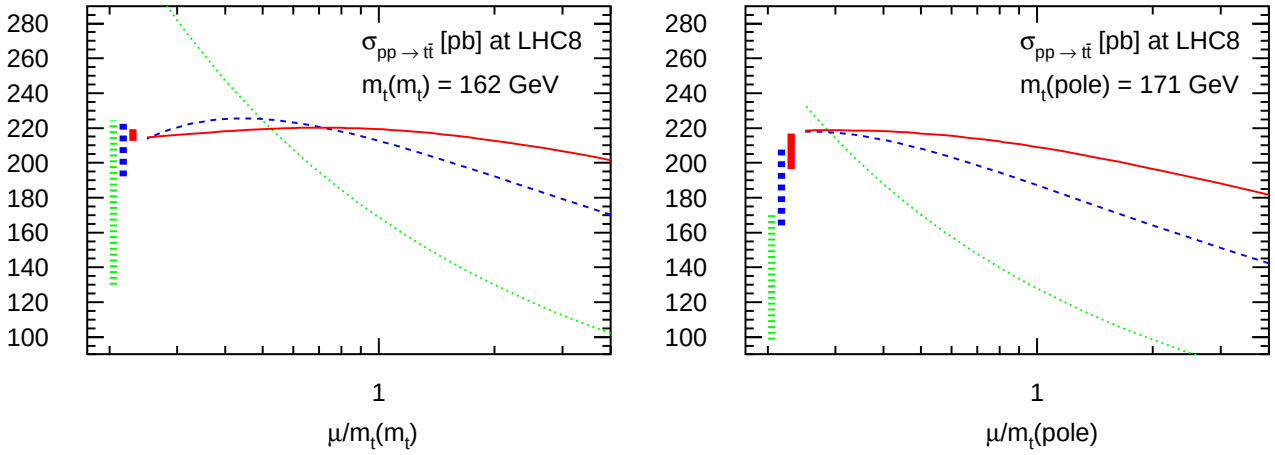

Figure 2.7: The scale dependence of the LO, NLO and NNLO QCD predictions for the $t\bar{t}$ total cross section at the LHC ($\sqrt{s}$ = 8 TeV) for a top-quark mass $m_t(m_t)$ = 162 GeV in the $\overline{\rm MS}$ scheme (left) and m_t(pole) = 171 GeV in the on-shell scheme (right) with the ABM12 PDFs and the choice $\mu = \mu_r = \mu_f$. The vertical bars indicate the size of the scale variation in the standard range μ/m_t(pole) $\in [1/2, 2]$ and $\mu/m_t(m_t) \in [1/2, 2]$, respectively.

$2m_t/\sqrt{s} \simeq 0.04 \ldots 0.05$ for the runs at $\sqrt{s}$ = 7 and 8 TeV c.m.s. energy, a region in x which is well constrained by data from the HERA collider, though.

The available data for the total $t\bar{t}$ cross section from ATLAS and CMS at $\sqrt{s}$ = 7 TeV [18, 19] and at $\sqrt{s}$ = 8 TeV [20–22] c.m.s. energy display good consistency, although, for the data sets at $\sqrt{s}$ = 7 TeV only within the combined uncertainties. Generally, the systematic and luminosity uncertainties dominate over the small statistical uncertainty and the CMS data [19, 21, 22] as well as the result from the Tevatron combination [23] are accurate to O(5%) while the ATLAS measurements [18, 20] have an error slightly larger than O(10%).

The QCD corrections for inclusive $t\bar{t}$-pair production are complete to NNLO [43–46], so that these data can be consistently added to the ABM11 PDF fit at NNLO. The theory predictions are available for the top-quark mass in the $\overline{\rm MS}$ scheme with $m_t(\mu_r)$ being the running mass [47] as well as for the pole mass m_t(pole) in the on-shell renormalization scheme [43–46]. The distinc-

tion is important, because the theory predictions as a function of the running mass $m_t(\mu_r)$ display much improved convergence and better scale stability of the perturbative expansion [47]. This is illustrated in Figs. 2.6 and 2.7 for the total $t\bar{t}$-cross section computed with the program `Hathor` (version 1.5) [48]. In Fig. 2.6 we show the size of the higher order perturbative corrections from LO to NNLO taking the PDFs order independent, i.e., the ABM11 set at NNLO, as a function of the top-quark mass for the LHC at $\sqrt{s} = 8$ TeV c.m.s. energy. Likewise, Fig. 2.7 illustrates the scale stability for two representative top-quark masses, $m_t(m_t) = 162$ GeV and $m_t(\text{pole}) = 171$ GeV. Figs. 2.6 and 2.7 imply a small residual theoretical uncertainty for the $t\bar{t}$-cross section predictions if expressed in terms of the running mass.

We have performed a variant of the ABM12 fit, adding the combined $t\bar{t}$ cross section data from LHC and Tevatron [18–23] to test the impact of these data on the gluon PDF, on the strong coupling α_s and on the value and scheme choice for the top-quark mass. It is strictly necessary to consider these three parameters together, since they are strongly correlated in theory predictions for the $t\bar{t}$-cross section at the LHC. In Figs. 2.8 and 2.9 we present the χ^2 profile versus the top-quark mass for the variants of the ABM12 fit with the $t\bar{t}$ cross section data included and for the two different top-quark mass definitions, i.e., the $\overline{\text{MS}}$ mass $m_t(m_t)$ and the pole mass $m_t(\text{pole})$. Fig. 2.8 displays a steeper χ^2 profile for the pole-mass definition. This implies a bigger impact of the $t\bar{t}$-cross section data in the fit and, as a consequence, greater sensitivity to the theoretical uncertainty at NNLO and uncalculated higher order corrections to the cross section beyond NNLO. In contrast, the χ^2 profile for the $\overline{\text{MS}}$ mass is markedly flatter. Fig. 2.9 shows the χ^2 profile for the subset of the $t\bar{t}$-cross section data with $NDP = 5$ and nicely demonstrates that a top-quark mass determination from the fit is feasible.

If one requires a $\Delta\chi^2_t = 1$, the value for the $\overline{\text{MS}}$ mass is obtained at NNLO

$$m_t(m_t) = 162.3 \pm 2.3 \text{ GeV}, \tag{2.4}$$

where we define the error in $m_t(m_t)$ due the experimental data, the PDFs and the value of $\alpha_s(M_Z)$ as the difference between the value for $m_t(m_t)$ at $\Delta\chi^2_t = 1$ and the minimum of the χ^2-profile in Fig. 2.9. The additional theoretical uncertainty from the variation of the factorization and renormalization scales in the usual range is small, $\Delta m_t(m_t) = \pm 0.7$ GeV, see Fig. 2.7 and [49]. Eq. (2.4) is equivalent to the top-quark pole mass value of

$$m_t(\text{pole}) = 171.2 \pm 2.4 \text{ GeV}, \tag{2.5}$$

using the known perturbative conversion relations [50–52]. Eq. (2.5) can be compared to the value of $m_t(\text{pole}) = 169.6 \pm 2.7$ GeV read off from Fig. 2.9. This indicates good consistency of the procedure and also with the top-quark mass values obtained from other determinations[2].

Having established the sensitivity to the value of the top-quark mass, we have performed further variants of the ABM12 fit by fixing $m_t(m_t)$ and $m_t(\text{pole})$ in order to quantify the impact on the gluon PDF and on α_s. The values for $\alpha_s(M_Z)$ which are obtained in these variants span the range $\alpha_s(M_Z) = 0.1133 \ldots 0.1142$ for $m_t(m_t) = 161 \ldots 163$ GeV and $\alpha_s(M_Z) = 0.1144 \ldots 0.1154$ for the range of $m_t(\text{pole}) = 171 \ldots 173.3$ GeV. The corresponding changes in the gluon PDF are illustrated in Fig. 2.10, which shows the relative change in the ABM12 gluon distribution at the factorization scale of $\mu = 3$ GeV in the 3-flavor scheme due to adding of the $t\bar{t}$-cross section data in the fit and fixing $m_t(m_t)$ and $m_t(\text{pole})$ to the values indicated. For the running-mass definition the changes in the gluon PDF are within the uncertainties of the nominal ABM12 fit. In particular, we find

[2] The values in Eqs. (2.4) and (2.5) supersede the top-quark mass determination in [49], because full account of the correlations among all non-perturbative parameters is kept.

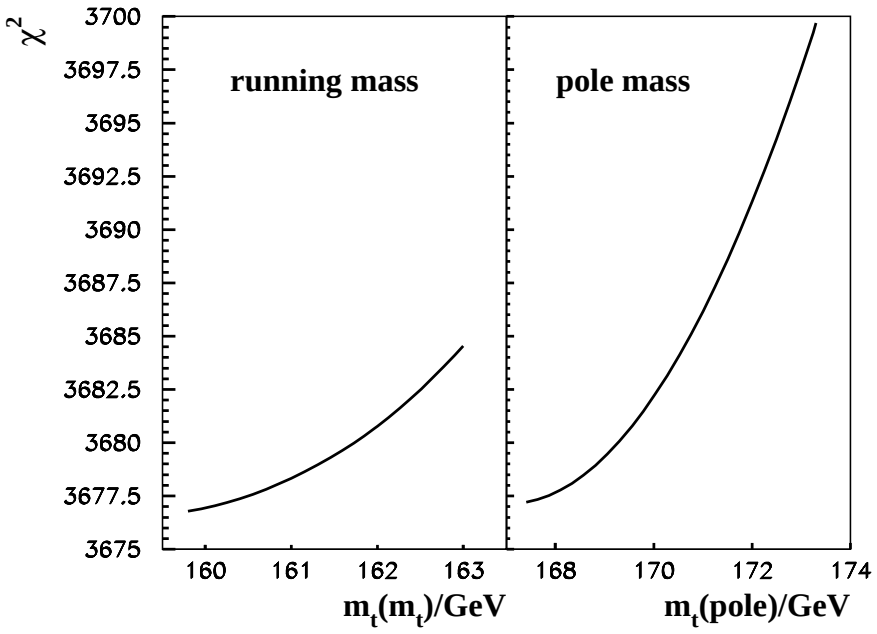

Figure 2.8: The χ^2 profile versus the t-quark mass for the variants of ABM12 fit with the $t\bar{t}$ cross section data included and different t-quark mass definitions: running mass (left) and pole mass (right).

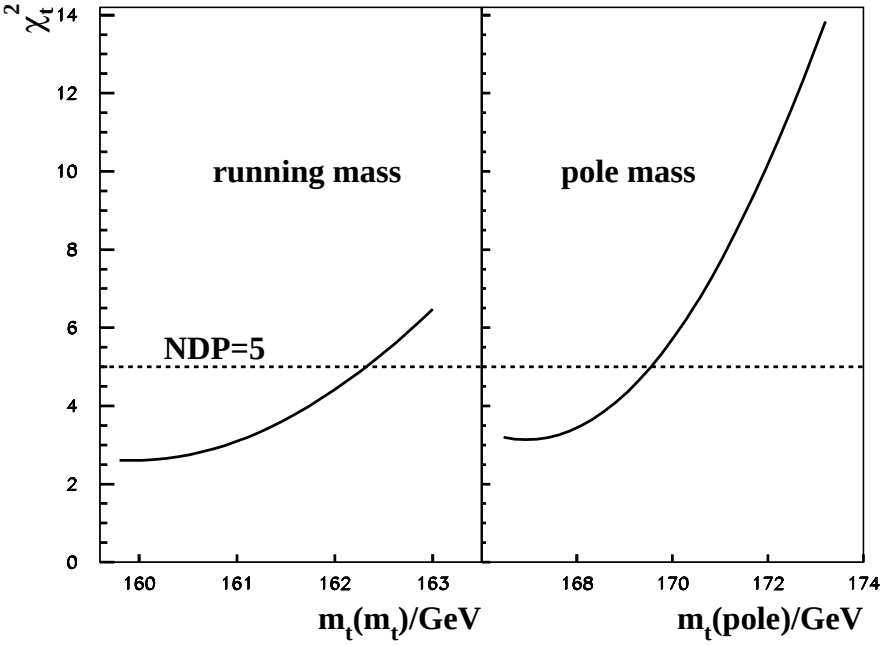

Figure 2.9: The same as in Fig. 2.8 for the $t\bar{t}$ cross section data subset. The $NDP = 5$ for this subset is displayed by the dashed line.

$\alpha_s(M_Z) = 0.1139(10)$ and a marginal change in the gluon PDF for a variant of ABM12 fit with $m_t(m_t) = 162$ GeV fixed and with the CMS [19, 21, 22] and the Tevatron [23] data included, i.e., leaving out the ATLAS data due to the larger experimental uncertainties. This is to be compared

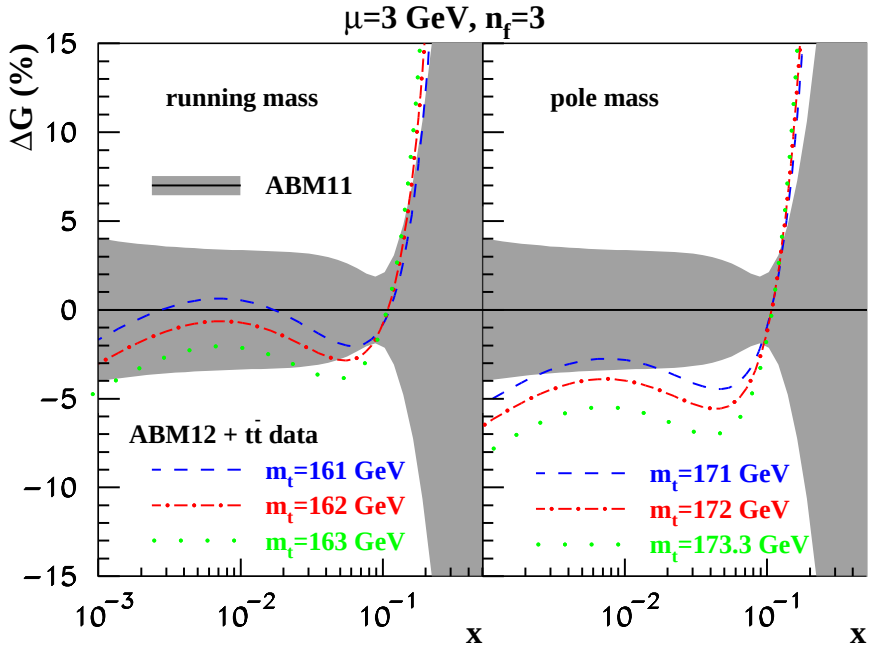

Figure 2.10: The relative uncertainty in the ABM12 gluon distribution in the 3-flavor scheme at the factorization scale of $\mu = 3$ GeV (grey area) in comparison to its relative change due to inclusion of the $t\bar{t}$ cross section data with the different mass definitions, running mass (left), pole mass (right), and the t-quark mass settings as indicated in the plot.

with $\alpha_s(M_Z) = 0.1133(8)$ for the ABM11 PDF fit and, again, demonstrates nicely the stability of the analysis, provided all correlations are accounted for.

We briefly comment here on related studies, that have appeared in the literature. Ref. [53] determines the strong coupling constant from a fit to $t\bar{t}$ cross section data and obtains the value of $\alpha_s(M_Z) = 0.1185(28)$ for the ABM11 PDFs with a fixed m_t(pole) = 173.2 GeV. Ref. [53] has used version 1.3 of `Hathor` [48], though, which returns a slightly different the central value (O(1%) change) for the cross section compared to version 1.5. The sensitivity to α_s is determined from fits to sets of PDFs for varying values of $\alpha_s(M_Z)$, i.e., using the ABM11 set at NNLO (`abm11_5n_as_nnlo.LHgrid` in the `LHAPDF` library [54, 55]) which covers the range $\alpha_s = 0.105 \ldots 0.12$. As a main caveat, the analysis of Ref. [53] misses the PDFs uncertainties for the PDF sets with varying values of $\alpha_s(M_Z)$ and the correlations of the parameters, i.e., the gluon PDF, α_s and m_t(pole) discussed above.

Ref. [56] explores the constraints on the gluon PDF from the same set of LHC and Tevatron $t\bar{t}$ cross section data [18–23] considered here. The analysis of Ref. [56] uses fixed values for α_s and the pole mass m_t(pole) and, thereby, disregards the correlation of these parameters with the gluon PDF. As illustrated in Fig. 2.10 this introduces a significant bias so that the fit results of Ref. [56] are a direct consequence of those assumptions. Ref. [56] also compares the ABM11 PDFs [6] to those data [18–23] and quotes a value of $\chi^2 = 40.2$ for $NDP = 5$ (Tab. 7 in Ref. [56]). Unfortunately, this computation of the χ^2-value is incomplete, since it is obtained by neglecting the PDF uncertainties, the uncertainty in the value of m_t(pole) as well as other uncertainties, which may have an impact on the χ^2-value such as the uncertainty in the beam energy, currently estimated to be 1%. The χ^2 profile in Fig. 2.9 shows that a faithful account of all sources of uncertainties and their correlation leads to a very good description of the $t\bar{t}$ cross section data.

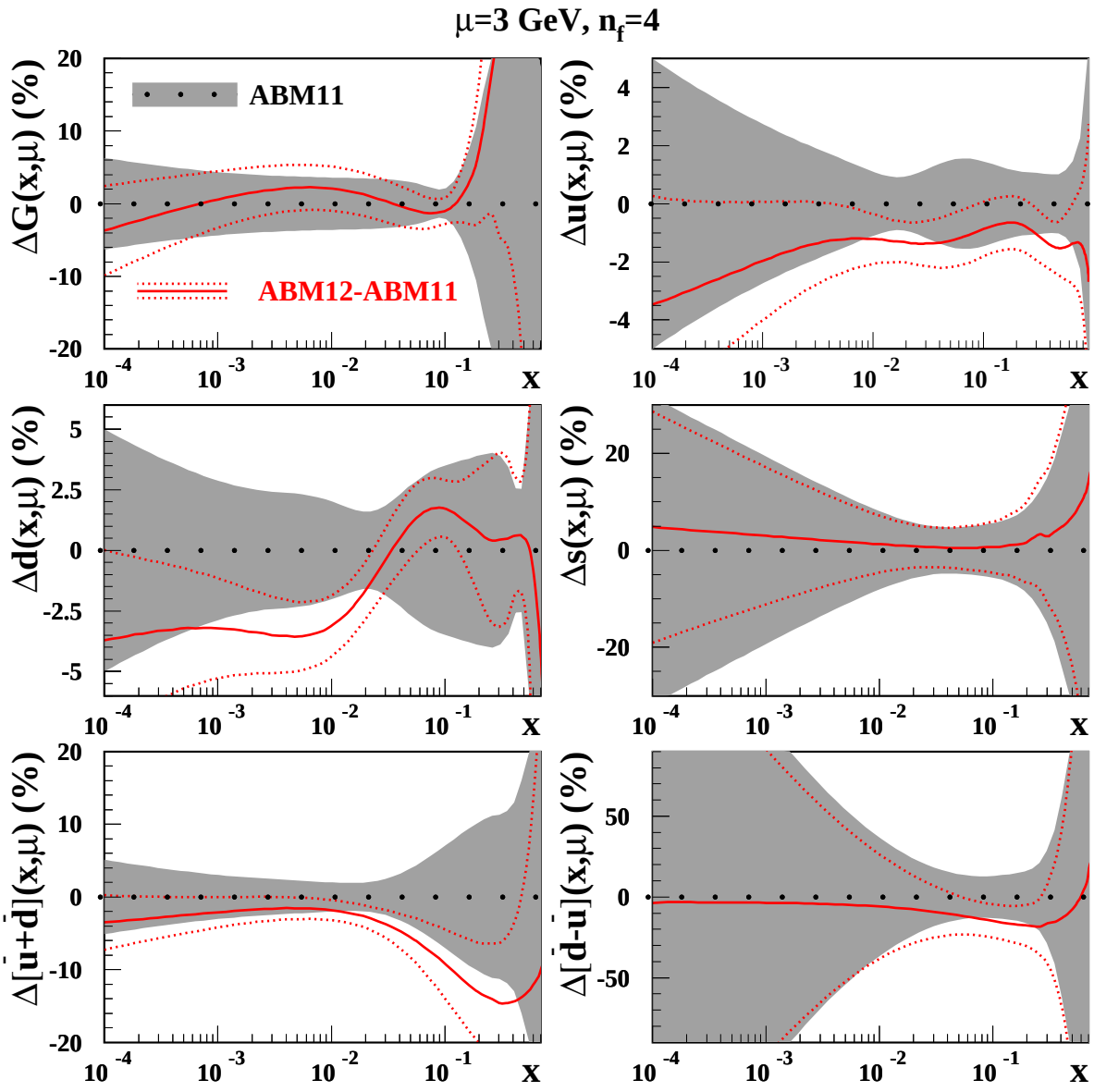

Figure 3.1: The 1σ band for the 4-flavor NNLO ABM11 PDFs [6] at the scale of $\mu = 3$ GeV versus x (shaded area) compared with the relative difference between ABM11 PDFs and the ABM12 ones obtained in this analysis (solid lines). The dotted lines display 1σ band for the ABM12 PDFs.

3 The ABM12 PDF results

In this Section the results of the ABM12 fit are discussed in detail and compared specifically with the previous ABM11 PDFs. Regarding the strong coupling constant $\alpha_s(M_Z)$ we also review the current situation for α_s-determinations from other processes, where the NNLO accuracy in QCD has been achieved. Finally, we apply the new ABM12 PDF grids in the format for the `LHAPDF` library [54, 55] to compute a number of benchmark cross sections at the LHC.

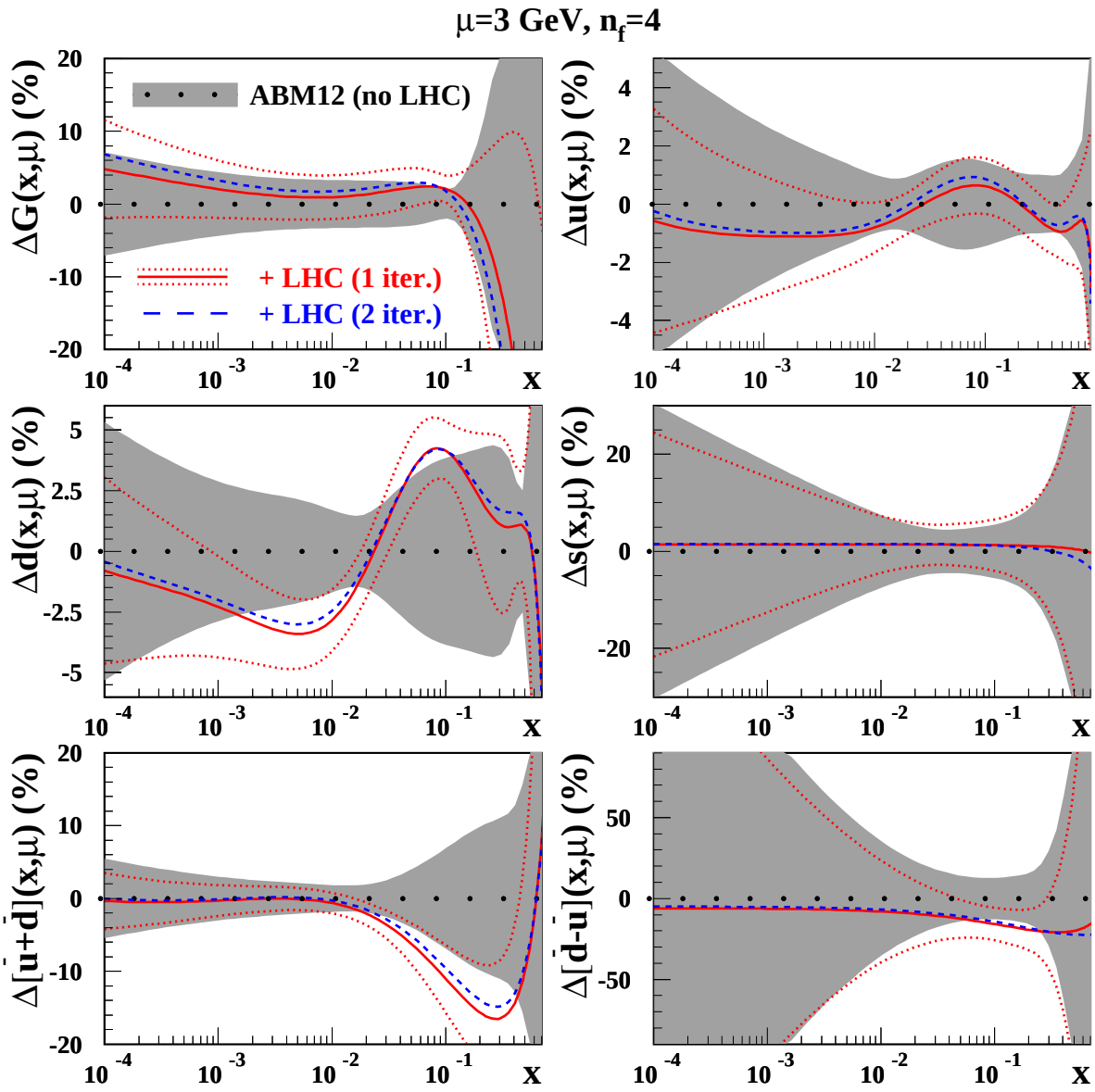

Figure 3.2: The same as in Fig. 3.1 for the 1σ band obtained in the variant of the ABM12 fit without the LHC DY data included (shaded area) and the relative change in the ABM12 PDFs due to the LHC DY data obtained with one (solid line) and two (dashes) iterations of the fast algorithm used to take into account the DY NNLO corrections. The dotted lines display 1σ band for the ABM12 PDFs obtained with one iteration of the algorithm.

3.1 Comparison with ABM11 and other PDFs

The PDFs obtained in the present analysis are basically in agreement with the ABM11 ones obtained in the earlier version of our fit [6] within the uncertainties, cf. Fig. 3.1. The strange quark distribution is particularly stable since in our analysis it is constrained by the neutrino-induced dimuon production that was not updated neither from the experimental nor from the theoretical side. It is still significantly suppressed as compared to the non-strange sea and this contrasts with the strangeness enhancement found in the ATLAS PDF analysis based on the collider data only [14]. The change in the gluon distribution happens in particular due to impact of the HERA

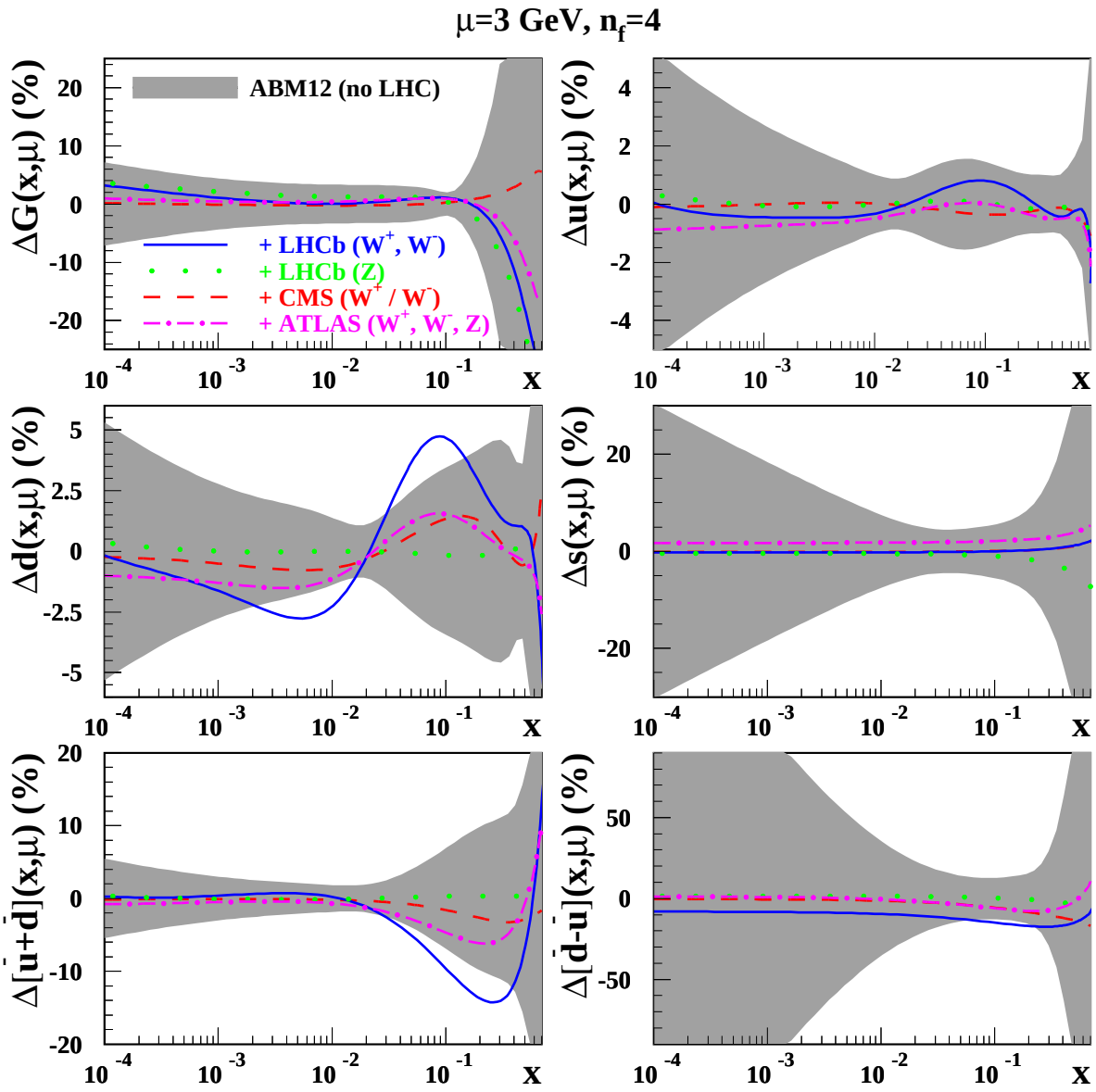

Figure 3.3: The same as in Fig. 3.2 for the variants of ABM12 fit including separate LHC DY data sets (sold line: LHCb [15], dots: LHCb [17], dashes: CMS [16], dashed dots: ATLAS [14]).

charm data and improvements in the heavy-quark electro-production description, cf. Ref. [33] for details. At the same time the ABM12 quark distributions differ from the ABM11 ones at most due to the LHC DY data. This input contributes to a better separation of the non-strange sea and the valence quark distributions. As a result, at the factorization scale $\mu = 3$ GeV and $x \sim 0.2$ the non-strange sea goes down by somewhat 15%, while the total d-quark distribution goes up by some 2%, cf. Fig. 3.2. In turn, this improvement allows for a better accuracy of both, the sea and the valence distributions, in particular, of the d-quark one. This improvement is particularly valuable since the accuracy of the latter is limited in the case of DIS data due to the uncertainty in the nuclear correction employed to describe the deuterium-target data. The LHCb data on W^+ and W^- production [15] provide the biggest impact on the PDFs as compared to other LHC data, cf. Fig. 3.3, due to the forward kinematics probed in this experiment. It is also worth noting that

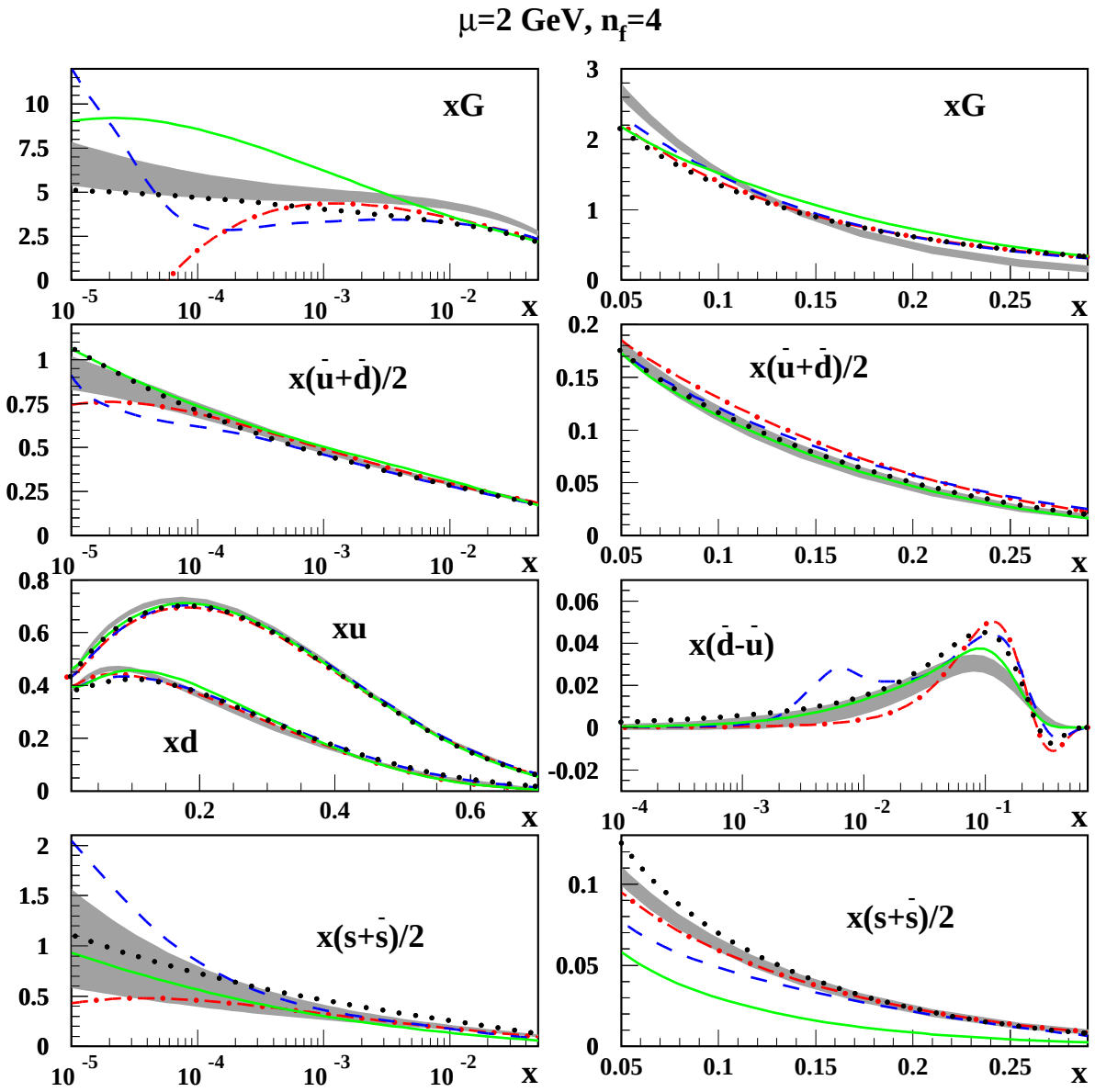

Figure 3.4: The 1σ band for the 4-flavor NNLO ABM12 PDFs at the scale of $\mu = 2$ GeV versus x obtained in this analysis (shaded area) compared with the ones obtained by other groups (solid lines: JR09 [57], dashed dots: MSTW [58], dashes: NN23 [59], dots: CT10 [60]).

the gluon distribution is also sensitive to the existing LHC DY data and in the ABM fit they pull it somewhat up (down) at small (large) x. However, in general, the changes are within the PDF uncertainties. This justifies our approach of using the set of PDF uncertainties to pre-calculate the NNLO DY cross-section grid and then to compute those cross sections by grid interpolation in minimal time. To provide the best accuracy of this algorithm the ABM12 PDFs are produced taking the DY cross-section grid calculated for the PDFs obtained in the variant of ABM12, which differs from the nominal ABM12 one by inclusion of the LHC data only. Furthermore, to check explicitly the stability of the algorithm we perform a second iteration of the fit based on the DY cross-section grids prepared with the PDFs obtained in the first iteration. The iterations demonstrate nice convergence and the first iteration suffices to obtain an accurate result, cf. Fig. 3.2.

The NNLO PDFs obtained in this analysis are compared to the results of other groups in Fig. 3.4. Our PDFs are in reasonable agreement with the newly released CT10 PDFs [60]. The most striking difference is observed for the large-x gluon distribution, which is constrained by the Tevatron jet data in the CT10 analysis. It is worth noting that this constraint is obtained for CT10 using the NLO corrections only, while the NNLO corrections may be as big as 15-25% [61]. Therefore the discrepancy between CT10 and our result should decrease once the NNLO corrections to the jet production are taken into account. Comparison of the ABM12 PDFs with the ones obtained by other groups demonstrate the trend similar to the ABM11 case [6]. The most essential difference appears in the large-x gluon distribution. It is also constrained by the Tevatron jet data for MSTW08 [58] and NN23 [59], with the NNLO corrections due to the threshold resummation taken into account in this case. However, the threshold resummation terms used in Refs. [58, 59] introduce additional theoretical uncertainties [62]. Therefore, a conclusive comparison with our results is still impractical. The spread in the small-x gluon distribution obtained by different groups can be consolidated with the help of the H1 data on the structure function F_L [63] being sensitive in this region. Similarly, differences in the estimates of the non-strange sea distribution at $x \sim 0.2$ can be eliminated using the LHC DY data considered in our analysis. At the same time the observed spread in the results for the strange sea shape cannot be explained by a particular data selection or difference in the theoretical accuracy of the analyses since all the groups use the CCFR and NuTeV data on the neutrino-induced dimuon production [64] as a strange sea constraint and take into account the NLO corrections to this process [65, 66]. The very recent precise data on the neutrino-induced dimuon production by NOMAD [67] are still not included in the present analysis. However, they demonstrate good agreement with the ABM11 prediction and may help to consolidate different estimates of the shape of the strange sea.

3.2 The strong coupling constant and the charm quark mass

The strong coupling constant $\alpha_s(M_Z)$ is measured together with the parameters of the PDFs, the heavy-quark mass m_c and the higher twist parameters within the analysis. The present accuracies of the scaling violations of the deep-inelastic world data make the use of NNLO QCD corrections mandatory. At NLO the scale uncertainties typically amount to $O(5\%)$, cf. [68], and, therefore, are simply too large.

The value of $\alpha_s(M_Z)$ obtained in the present analysis is

$$\alpha_s^{\rm NNLO}(M_Z) \;=\; 0.1132 \pm 0.0011\,. \tag{3.1}$$

This result is in excellent agreement with those given by other groups and by us in Refs. [5, 6, 57, 69–71], see Tab. 3.1. As has been shown in [6] in detail the α_s-values obtained upon analyzing the partial data sets from BCDMS [72, 73], NMC [74, 75], SLAC [76–81], HERA [13], and the Drell-Yan data [82, 83] both at NLO and NNLO do very well compare to each other and to the central value within the experimental errors.

Fits including jet data have been carried out before both by JR [84] and ABM [6, 85], along with other groups, performing systematic studies including both jet data from the Tevatron and in [6] also from LHC [3]. We would like to note that it is very problematic to call present NNLO fits of the world DIS data including jet data NNLO analyses, since the corresponding jet scattering cross sections are available at NLO *only*. The complete NNLO results for the corresponding jet

[3] Contrary statements given in Refs. [86, 87] are incorrect; see Ref. [6] for further details.

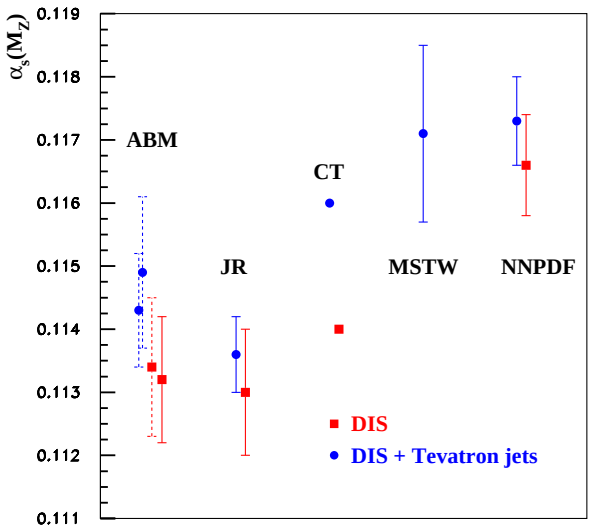

Figure 3.5: The values of $\alpha_s(M_Z)$ at NNLO obtained in the PDF fits of ABM (solid bars: this analysis, dashed bars: ABM11 [6]) in comparison with the CT [60], JR [57], MSTW [58] and NNPDF [88] results.

cross sections have to be used in later analyses, since threshold resummations are not expected to deliver a sufficient description [62] [4].

The $\alpha_s(M_Z)$ values for some PDF groups are illustrated in Fig. 3.5. In Tab. 3.1 a general overview on the values of $\alpha_s(M_Z)$ at NNLO is given, with a few determinations effectively at N^{3}LO in the valence analyses [69, 70], and the hadronic Z-decay [89]. The BBG, BB, GRS, ABKM, JR, ABM11, CTEQ analyses and the present analysis find lower values of $\alpha_s(M_Z)$ with errors at the 1–2% level, while NN21 and MSTW08 find larger values analyzing the deep-inelastic world data, Drell-Yan data, and partly also jet data with comparable accuracy to the former ones.[5] Reasons for the higher values being obtained by NN21 and MSTW08 were given in [6] before. As has been shown in [91] a consistent F_L-treatment for the NMC data and the BCDMS-data, cf. [69], is necessary and leads to a change of the value of $\alpha_s(M_Z)$ to lower values. Furthermore, the sensitivity on kinematic cuts applied to remove higher twist effects has been studied. In the flavor non-singlet case this can be achieved by cutting for $W^2 > 12.5$ GeV^2, cf. [69]. In the singlet analysis there are also higher twist contributions in the lower x-region to be removed by applying the additional cut of $Q^2 > 10$ GeV^2, which, however, is not used by NN21 and MSTW08. We performed a fit without accounting for the higher twist terms and allowed for the range of data down to values of $Q^2 > 2.5$ GeV^2 at $W^2 > 12.5$ GeV^2, [6]. One obtains $\alpha_s(M_Z) = 0.1191 \pm 0.0016$, very close to the values found by NN21 and MSTW08. Comparisons of the α_s values in the fits by NN21 and MSTW08, furthermore, show strong variations with respect to different DIS data sets [6], despite of the similar final value.

The analyses of thrust in e^+e^- data by two groups also find low values, also with errors at the 1% level. Higher values of $\alpha_s(M_Z)$ are obtained for the e^+e^- 3-jet rate, the hadronic Z-decay, and τ-decay within various analyses. The value of $\alpha_s(M_Z)$ has also been determined in different lattice simulations to high accuracy. The N^{3}LO values for $\alpha_s(M_Z)$ in the valence analyses [69, 70] yield slightly larger values than at NNLO. They are fully consistent with the NNLO values within errors.

[4] Partial NNLO results on the hadronic di-jet cross section are available [61].

[5] Very recently MSTW [90] reported lower values for $\alpha_s(M_Z)$ also related to the LHC data.

The corresponding shift can be taken as a measure for the remaining theoretical uncertainty in the non-singlet-case, see Tab. 3.1.

Finally we would like to comment on recent determinations of $\alpha_s(M_Z)$ at NLO using the jet data [92, 93]. The ATLAS and CMS jet data span a wider kinematic range than those of Tevatron and will allow very soon even more accurate measurements. In the analysis [93] $\alpha_s(M_Z)$ is determined scanning grids generated at different values of the strong coupling constants by the different PDF-fitting groups. These are used to find a minimum for the jet data. Including the scale uncertainties the following NLO values are obtained for the 3/2 jet ratio by CMS [93] :

$$\alpha_s(M_Z) = 0.1148 \pm 0.0014\,(\text{exp.}) \pm 0.0018\,(\text{PDF}) \,^{+0.0050}_{-0.0055}\,(\text{scale})\;\; \text{NNPDF21}\;\; [94], \tag{3.2}$$

$$\alpha_s(M_Z) = 0.1135 \pm 0.0018\,(\text{exp.})\;\; [0.180\;(\text{favored value})]\;\; \text{CT10}\;\; [60], \tag{3.3}$$

$$\alpha_s(M_Z) = 0.1141 \pm 0.0022\,(\text{exp.})\;\; [0.1202\;^{+0.0012}_{-0.0015}\;]\;\; \text{MSTW08}\;\; [95]. \tag{3.4}$$

A comparable NLO value has been reported using ATLAS jet data [92]

$$\alpha_s(M_Z) = 0.1151 \pm 0.0050\,(\text{exp.})\;^{+0.0080}_{-0.0073}\;(\text{th.})\,. \tag{3.5}$$

Interestingly, rather low values are obtained already at NLO. In parenthesis we quote the NLO values for $\alpha_s(M_Z)$ in Eqs. (3.2)-(3.4) which are obtained by the fitting groups at minimal χ^2. Obviously the values found in the jet-data analysis do not correspond to these values. Yet, the NLO scale uncertainty in this analysis is large. Recently the jet energy-scale error has been improved by CMS [93], leading to a significant reduction of the experimental error. The gluonic NNLO K-factor is positive; as shown in Fig. 2 of Ref. [61] the scale dependence for $\mu = \mu_F = \mu_R$ behaves flat over a wide range of scales. It is therefore expected that also the error due to scale variation will turn out to be very small in the NNLO analysis. It will be important to repeat this analysis and to fit the LHC jet data together with the world deep-inelastic data, which will be also instrumental for the determination of the gluon distribution at large scales.

The present DIS world data together with the $F_2^{c\bar{c}}(x, Q^2)$ data, are competitive in the determination of the charm quark mass in a correlated fit with the PDF-parameters and $\alpha_s(M_Z)$. For the $\overline{\text{MS}}$ mass the value of

$$m_c(m_c) = 1.24 \pm 0.03\,(\text{exp.})\;^{+0.04}_{-0.00}\;(\text{th.})\;\text{GeV} \tag{3.6}$$

is obtained at NNLO, see also [33]. At present this analysis is the only one, in which all known higher order heavy-flavor corrections to deep-inelastic scattering have been considered. This value still should be quoted as of approximate NNLO, since the NNLO-corrections are only modeled [26] combining small-x and threshold resummation effects with information of the 3-loop moments of the heavy-flavor Wilson coefficients [31] at high values of Q^2. Two scenarios have been considered in [26] to parameterize the Wilson coefficients accounting for an estimated error. Here the fit favors a region of the parameter $d_N \in [-0.1, 0.5]$, cf. [26], on which the theoretical error is based [6]. The value in Eq. (3.6) compares well to the present world average of $m_c(m_c) = 1.275 \pm 0.025$ GeV [1].

It is needless to say that the determination of a fundamental parameter of the SM, such as m_c, has to follow a thorough quantum field-theoretic prescription, rather than specific models also

[6] The calculation of the exact NNLO heavy-flavor Wilson coefficients is underway [32, 109–111].

	$\alpha_s(M_Z)$	
BBG	$0.1134\ ^{+\ 0.0019}_{-\ 0.0021}$	valence analysis, NNLO [69]
BB	0.1132 ± 0.0022	valence analysis, NNLO [70]
GRS	0.112	valence analysis, NNLO [71]
ABKM	0.1135 ± 0.0014	HQ: FFNS $n_f = 3$ [5]
ABKM	0.1129 ± 0.0014	HQ: BSMN-approach [5]
JR	0.1128 ± 0.0010	dynamical approach [96]
JR	0.1140 ± 0.0006	including jet data [96]
ABM11	0.1134 ± 0.0011	[6]
ABM12	0.1132 ± 0.0011	Eq. (3.1) this work
MSTW	0.1171 ± 0.0014	[95]
MSTW	$0.1155 - 0.1175$	[90]
NN21	0.1173 ± 0.0007	[88]
CTEQ	0.1159...0.1162	[60]
CTEQ	0.1140	(without jets) [60]
BBG	$0.1141\ ^{+\ 0.0020}_{-\ 0.0022}$	valence analysis, N^{3}LO(*) [69]
BB	0.1137 ± 0.0022	valence analysis, N^{3}LO(*) [70]
e^+e^- thrust	0.1140 ± 0.0015	Abbate et al. [97]
e^+e^- thrust	$0.1131\ ^{+\ 0.0028}_{-\ 0.0022}$	Gehrmann et al. [98]
3 jet rate	0.1175 ± 0.0025	Dissertori et al. 2009 [99]
Z-decay	0.1189 ± 0.0026	BCK 2008/12, N^{3}LO [89, 100]
τ decay	0.1212 ± 0.0019	BCK 2008 [100]
τ decay	0.1204 ± 0.0016	Pich 2011 [101]
τ decay	0.1191 ± 0.0022	Boito et al. 2012 [102]
lattice	0.1205 ± 0.0010	PACS-CS 2009 (2+1 fl.) [103]
lattice	0.1184 ± 0.0006	HPQCD 2010 [104]
lattice	0.1200 ± 0.0014	ETM 2012 (2+1+1 fl.) [105]
lattice	0.1156 ± 0.0022	Brambilla et al. 2012 (2+1 fl.) [106]
lattice	0.1181 ± 0.0014	JLQCD [107]
world average	0.1184 ± 0.0007	Bethke 2012 [108]

Table 3.1: Summary of recent NNLO and N^{3}LO QCD analyses of the DIS world data, supplemented by related measurements using a series of other processes and lattice determinations. In case that jet data from hadron colliders are used in the analysis the values of $\alpha_s(M_Z)$ cannot be considered NNLO values.

being found in the literature, cf., e.g. [112]. Despite the correct renormalization procedure of the

heavy-flavor Wilson coefficients to 3-loop order were known [31] to 3-loop order, there are still even massless scenarios to this level, cf. e.g. [113], which ignore the exact theoretical description.

3.3 Standard candle cross sections

In this Section we quantify the impact of the new PDF set on the predictions for benchmark cross sections at the LHC for various c.m.s. energies. To that end, we confine ourselves to (mostly) inclusive cross sections which are known to NNLO in QCD, see [6, 7] for previous benchmark numbers, since the NNLO accuracy is actually the first instance, where meaningful statements about the residual theoretical uncertainty are possible given the precision of present collider data and the generally large residual variation of the renormalization and factorization scale at NLO.

In detail, we consider the following set of inclusive observables at NNLO in QCD: hadronic W- and Z-boson production [114, 115], the cross section for Higgs boson production in gluon-gluon fusion [115–118], and the cross section for top-quark pair production [43–47]. We have used the `LHAPDF` library [54, 55] for the cross section computations to interface to our PDFs provided in the form of data grids for $n_f = 3, 4$ and 5 flavors accessible with the `LHAPDF` library [7],

```
abm12lhc_3_nnlo.LHgrid (0+28),
abm12lhc_4_nnlo.LHgrid (0+28),
abm12lhc_5_nnlo.LHgrid (0+28),
```

which contains the central fit and 28 additional sets for the combined symmetric uncertainty on the PDFs, on α_s and on the heavy-quark masses. All PDF uncertainties quoted here are calculated in the standard manners, i.e., as the $\pm 1\sigma$-variation.

3.3.1 W- and Z-boson production

We start by presenting results for W- and Z-boson production at the LHC. For the electroweak parameters, we follow [6,7] and choose the scheme based on the set (G_F, M_W, M_Z). According to [1], we have $G_F = 1.16638 \times 10^{-5}$ GeV^{-2}, $M_W = 80.385 \pm 0.015$ GeV, $M_Z = 91.1876 \pm 0.0021$ GeV and the corresponding widths $\Gamma(W^{\pm}) = 2.085 \pm 0.042$ GeV and $\Gamma(Z) = 2.4952 \pm 0.0023$ GeV. The weak mixing angle is then a dependent quantity, with

$$\hat{s}_Z^2 \;=\; 1 - \frac{M_W^2}{\hat{\rho} M_Z^2} = 0.23098 \pm 0.00041\,, \tag{3.7}$$

and $\hat{\rho} = 1.01051 \pm 0.00011$. The Cabibbo angle θ_c yields the value of $\sin^2\theta_c = 0.05085$.

The change in the predictions between ABM11 and ABM12 is small and for the current theoretical accuracy, the uncertainty due to the scale variation is already significantly smaller compared to the PDF error, see Tabs. 3.2–3.5. This indicates the very good stability of the PDF fit and the consistency of the previous ABM11 PDFs with the new variant including LHC data. An additional source of theoretical uncertainty for W- and Z-boson production, namely the choice of PDF sets with $n_f = 4$ or with $n_f = 5$ flavors (as in Tabs. 3.2–3.5) has already been discussed and quantified in [6]. Generally, those differences are less than 1σ in the PDF uncertainty and become successively smaller as perturbative corrections of higher order are included.

[7] The `LHAPDF` library can be obtained from `http://projects.hepforge.org/lhapdf` together with installation instructions.

LHC7	W^+	W^-	$W^\pm$	Z
ABM11	$59.53\ ^{+0.38\ +0.88}_{-0.23\ -0.88}$	$39.97\ ^{+0.28\ +0.65}_{-0.17\ -0.65}$	$99.51\ ^{+0.69\ +1.43}_{-0.41\ -1.43}$	$29.23\ ^{+0.18\ +0.42}_{-0.10\ -0.42}$
ABM12	$58.40\ ^{+0.38\ +0.70}_{-0.24\ -0.70}$	$39.63\ ^{+0.29\ +0.45}_{-0.18\ -0.45}$	$98.03\ ^{+0.67\ +1.13}_{-0.41\ -1.13}$	$28.79\ ^{+0.17\ +0.33}_{-0.11\ -0.33}$

Table 3.2: The total cross sections [pb] for gauge boson production at the LHC with $\sqrt{s} = 7$ TeV for the $n_f = 5$ flavor PDF sets ABM11 and ABM12 at NNLO accuracy. The errors shown are the scale uncertainty based on the shifts $\mu = M_{W/Z}/2$ and $\mu = 2M_{W/Z}$ and, respectively, the 1σ PDF uncertainty.

LHC8	W^+	W^-	$W^\pm$	Z
ABM11	$68.30\ ^{+0.48\ +1.02}_{-0.29\ -1.02}$	$46.67\ ^{+0.35\ +0.748}_{-0.22\ -0.748}$	$114.97\ ^{+0.82\ +1.67}_{-0.51\ -1.67}$	$33.97\ ^{+0.23\ +0.50}_{-0.13\ -0.50}$
ABM12	$67.03\ ^{+0.48\ +0.81}_{-0.30\ -0.81}$	$46.27\ ^{+0.35\ +0.53}_{-0.23\ -0.53}$	$113.29\ ^{+0.84\ +1.32}_{-0.52\ -1.32}$	$33.49\ ^{+0.22\ +0.38}_{-0.14\ -0.38}$

Table 3.3: The same as Tab. 3.2 for the LHC with $\sqrt{s} = 8$ TeV.

LHC13	W^+	W^-	$W^\pm$	Z
ABM11	$110.77\ ^{+0.97\ +1.70}_{-0.61\ -1.70}$	$80.02\ ^{+0.72\ +1.28}_{-0.47\ -1.28}$	$190.79\ ^{+1.68\ +2.87}_{-1.09\ -2.87}$	$57.62\ ^{+0.48\ +0.88}_{-0.29\ -0.88}$
ABM12	$108.86\ ^{+0.97\ +1.39}_{-0.62\ -1.39}$	$79.33\ ^{+0.73\ +0.95}_{-0.48\ -0.95}$	$188.19\ ^{+1.69\ +2.31}_{-1.09\ -2.31}$	$56.88\ ^{+0.48\ +0.69}_{-0.29\ -0.69}$

Table 3.4: The same as Tab. 3.2 for the LHC with $\sqrt{s} = 13$ TeV.

LHC14	W^+	W^-	$W^\pm$	Z
ABM11	$119.03\ ^{+1.07\ +1.83}_{-0.68\ -1.83}$	$86.63\ ^{+0.80\ +1.39}_{-0.53\ -1.39}$	$205.66\ ^{+1.87\ +3.12}_{-1.20\ -3.12}$	$62.31\ ^{+0.53\ +0.96}_{-0.32\ -0.96}$
ABM12	$116.99\ ^{+1.07\ +1.51}_{-0.69\ -1.51}$	$85.89\ ^{+0.80\ +1.04}_{-0.53\ -1.04}$	$202.88\ ^{+1.87\ +2.52}_{-1.22\ -2.52}$	$61.52\ ^{+0.53\ +0.75}_{-0.33\ -0.75}$

Table 3.5: The same as Tab. 3.2 for the LHC with $\sqrt{s} = 14$ TeV.

3.3.2 Higgs boson production

Let us now discuss the cross section for the SM Higgs boson production in the gluon-gluon fusion channel, which is predominantly driven by the gluon PDF and the value of $\alpha_s(M_Z)$ from the effective vertex. The known NNLO QCD corrections [115–118] still lead to a sizable increase in

	LHC7	LHC8	LHC13	LHC14
ABM11	$13.23\ ^{+1.35\ +0.30}_{-1.31\ -0.30}$	$16.99\ ^{+1.69\ +0.37}_{-1.63\ -0.37}$	$39.57\ ^{+3.60\ +0.77}_{-3.42\ -0.77}$	$44.68\ ^{+4.02\ +0.85}_{-3.78\ -0.85}$
ABM12	$13.28\ ^{+1.35\ +0.31}_{-1.32\ -0.31}$	$17.05\ ^{+1.68\ +0.39}_{-1.64\ -0.39}$	$39.69\ ^{+3.60\ +0.84}_{-3.42\ -0.84}$	$44.81\ ^{+4.01\ +0.94}_{-3.80\ -0.94}$

Table 3.6: The total Higgs production cross sections [pb] in gluon-gluon fusion for the PDF sets ABM11 and ABM12 at NNLO accuracy using a Higgs boson mass $m_H = 125$ GeV. The errors shown are the scale uncertainty based on the shifts $\mu = m_H/2$ and $\mu = 2m_H$ and, respectively, the 1σ PDF uncertainty.

	LHC7	LHC8	LHC13	LHC14
HiggsXSWG [119]	$15.13\ ^{+1.07\ +1.15}_{-1.18\ -1.07}$	$19.27\ ^{+1.39\ +1.45}_{-1.50\ -1.33}$	–	$49.85\ ^{+6.08\ +3.69}_{-4.19\ -3.09}$

Table 3.7: The total Higgs production cross sections [pb] in gluon-gluon fusion of [119] used by ATLAS and CMS for a Higgs boson mass $m_H = 125$ GeV. The errors shown are the scale uncertainty and, respectively, the PDF+α_s uncertainty.

the cross section at nominal values of the scale, i.e. $\mu = m_H$, and it is well established that a further stabilization beyond NNLO may be achieved on the basis of soft gluon resummation, see e.g., [120]. At NNLO accuracy in QCD the theoretical uncertainty from the scale variation is dominating by far over the PDF uncertainty. Using a Higgs boson mass $m_H = 125$ GeV in Tab. 3.6 we observe again only rather small changes between the ABM11 and the ABM12 predictions. This demonstrates that the gluon PDF is well constrained from existing data and that the ABM11 results are consistent with the new fit based on including selected LHC ones.

It is therefore interesting to compare the ABM predictions in Tab. 3.6 to the cross section values recommended for use in the ongoing ATLAS and CMS Higgs analyses [119], cf., Tab. 3.7 [8]. The central values of the ABM predictions are significantly lower by some 11-14 %. Only a small fraction of this difference can be attributed to the inclusion of soft gluon resummation beyond NNLO, which typically does reduce the scale dependence, though, as is obvious from Tab. 3.7, and to the inclusion of other quantum corrections in [119], e.g., the electro-weak ones. Much larger sensitivity of the Higgs cross section predictions arise from theory assumptions made in the analyses, e.g., for constraints from higher orders in QCD due to the treatment of fixed-target DIS data, see [91]. The most interesting aspect is the fact, that the PDFs+α_s error in [119] is inflated roughly by a factor of 4 in comparison to our predictions in Tab. 3.6, where we quote the 1σ PDF (and α_s of course) error entirely determined from the correlated experimental uncertainties in the fitted data. In summary, the cross section predictions [119] used in the current Higgs analyses at the LHC are subject to both, a bias due to specific theory assumptions made in PDF and α_s fits as well as largely overestimated uncertainties of the relevant non-perturbative input. Thus, checks of correlations between experimental data for different scattering processes at the LHC and their sensitivity to PDFs along the lines of Sec. 2 are urgently needed to consolidate this issue, cf. [121].

3.3.3 Top-quark pair production

Finally, we present predictions for the total cross section for $t\bar{t}$-pair hadro-production in Tabs. 3.8 and 3.9. Using the program `Hathor` (version 1.5) [48] which incorporates the recently completed QCD corrections at NNLO [43–46], we give numbers for two representative top-quark masses, that is the running mass $m_t(m_t) = 162$ GeV in the $\overline{\rm MS}$ mass scheme and the pole mass $m_t(\text{pole}) = 171$ GeV in the on-shell scheme.

At NNLO accuracy in QCD, the PDF uncertainties given in Tabs. 3.8 and 3.9 are dominating in comparison to the theory uncertainties based on scale variation. As discussed at length in Sec. 2.4 the LHC data for $t\bar{t}$-pair production included in the ABM12 fit predominantly constrains the top-quark mass and has little impact on the gluon PDF and on the value of the strong coupling constant $\alpha_s(M_Z)$. Therefore the cross section predictions of the ABM11 and ABM12 PDFs largely coincide.

[8] See also `https://twiki.cern.ch/twiki/bin/view/LHCPhysics/CERNYellowReportPageAt7TeV` for details.

	LHC7	LHC8	LHC13	LHC14
ABM11	$141.6\ ^{+5.5\ +6.9}_{-8.7\ -6.9}$	$207.2\ ^{+7.8\ +9.3}_{-12.5\ -9.3}$	$727.6\ ^{+24.4\ +23.7}_{-39.4\ -23.7}$	$867.8\ ^{+28.5\ +27.0}_{-46.3\ -27.0}$
ABM12	$143.0\ ^{+5.6\ +6.5}_{-8.8\ -6.5}$	$209.1\ ^{+7.9\ +8.7}_{-12.6\ -8.7}$	$732.2\ ^{+24.4\ +22.9}_{-39.6\ -22.9}$	$872.9\ ^{+28.6\ +26.2}_{-46.3\ -26.2}$

Table 3.8: The total cross section for top-quark pair-production at NNLO [pb] using a pole mass $m_t(\text{pole}) = 171$ GeV and the PDF sets ABM11 and ABM12 and with the errors shown as $\sigma + \Delta\sigma_{\text{scale}} + \Delta\sigma_{\text{PDF}}$. The scale uncertainty $\Delta\sigma_{\text{scale}}$ is based on maximal and minimal shifts for the choices $\mu = m_t(\text{pole})/2$ and $\mu = 2m_t(\text{pole})$ and $\Delta\sigma_{\text{PDF}}$ is the 1σ combined PDF+α_s error.

	LHC7	LHC8	LHC13	LHC14
ABM11	$148.6\ ^{+0.2\ +6.6}_{-4.5\ -6.6}$	$217.2\ ^{+0.2\ +8.8}_{-6.5\ -8.8}$	$760.0\ ^{+0.0\ +22.2}_{-21.0\ -22.2}$	$906.0\ ^{+0.0\ +25.2}_{-24.7\ -25.2}$
ABM12	$150.2\ ^{+0.1\ +6.1}_{-4.6\ -6.1}$	$219.3\ ^{+0.1\ +8.2}_{-6.6\ -8.2}$	$765.1\ ^{+0.0\ +21.3}_{-21.1\ -21.3}$	$911.6\ ^{+0.0\ +24.4}_{-24.7\ -24.4}$

Table 3.9: The same as Tab. 3.8 for a running mass $m_t(m_t) = 162$ GeV in the $\overline{\text{MS}}$ scheme.

4 Conclusions

We have presented the PDF set ABM12, which results from a global analysis of DIS and hadron collider data including, for the first time, the available LHC data for the standard candle processes such as $W^{\pm}$- and Z-boson and $t\bar{t}$-production. The analysis has been performed at NNLO in QCD and along with the new data included also progress in theoretical predictions has been reflected accordingly. The new ABM12 analysis demonstrates very good consistency with the previous PDF sets (ABM11, ABKM09) regarding the parameter values for PDFs as well as the strong coupling constant $\alpha_s(M_Z)$ and the quark masses. Continuous checks for the compatibility of the data sets along with a detailed account of the systematic errors and of the correlations among the fit parameters have been of paramount importance in this respect.

In detail, we have considered new HERA data sets on semi-inclusive charm production in DIS in Sec. 2.1 which have allowed to validate the c-quark production mechanism in the FFN scheme relying on 3 light flavors in the initial state and leading to a precise determination of the running c-quark mass. As another new DIS data set, the neutral-current inclusive data at high Q^2 from HERA has been included, which exhibits sensitivity to the exchange of photons, Z-bosons as well as to γ-Z-interference. Our analysis in Sec. 2.2 corroborates again the fact, that even at high scales the FFN scheme is sufficient for description of the DIS data.

The fit of LHC precision data on $W^{\pm}$- and Z-boson production improves the determination on the quark distributions at $x \sim 0.1$ and constrains especially the d-quark distribution. The fit shows good consistency and a further reduction of the experimental systematic uncertainties would certainly strengthen the impact of the LHC DY data in global fits. On the technical side, we remark that the fit of DY data has been based on the exact NNLO differential cross section predictions, expanded over the set of eigenfunctions spanning the basis for the ABM PDF uncertainties. This has served as a starting point for a rapidly converging fit including the LHC DY data with account of all correlations.

Also data for the total $t\bar{t}$-cross section has been smoothly accommodated into the fit. A proper treatment of the correlation between the gluon PDF, the strong coupling constant $\alpha_s(M_Z)$ and the top-quark mass has been crucial here. Moreover, the running-mass definition for the top-

quark provides a better description of data as compared to the pole mass case, the latter showing still sizable sensitivity to perturbative QCD corrections beyond NNLO accuracy. Our analysis in Sec. 2.4 yields a precise value with an uncertainty of roughly 1.5 % for the $\overline{\rm MS}$ mass $m_t(m_t)$ which has been used to extract m_t(pole) at NNLO.

In summary, the new ABM12 fit demonstrates, that a smooth extension of the ABM global PDF analysis to incorporate LHC data is feasible and does not lead to large changes in the fit results. As we have shown in Sec. 3.1 differences with respect to other PDFs sets remain. However, these differences are based either on a different treatment of the data sets or on different theoretical descriptions of the underlying physical processes and we have commented on the correctness of some of those procedures. In particular, the value of strong coupling constant $\alpha_s(M_Z)$ in our analysis remains largely unchanged as documented in Sec. 3.2 and the theoretical predictions for benchmark cross section at the LHC are very stable. This particularly applies to the cross section for Higgs production in the gluon-gluon fusion shown in Sec. 3.3. We commented on the implications for the ongoing Higgs analyses at the LHC.

The precision of the currently available experimental data make global analyses at NNLO accuracy in QCD mandatory. This offers the great opportunity for high precision determinations of the non-perturbative parameters relevant in theory predictions of hadron collider cross section. At the same time, the great sensitivity to the underlying theory allows to test and to scrutinize remaining model prescriptions and, eventually, to reject wrong assumptions.

Acknowledgments

We would like to thank H. Böttcher for discussions, P. Jimenez-Delgado and E. Reya for a private communication prior to publication. We gratefully acknowledge the continuous support of M. Whalley to integrate the results of the new ABM fit into the `LHAPDF` library [54, 55].

J.B. acknowledges support from Technische Universität Dortmund. This work has been supported by Helmholtz Gemeinschaft under contract VH-HA-101 (*Alliance Physics at the Terascale*), by Deutsche Forschungsgemeinschaft in Sonderforschungsbereich/Transregio 9, by Bundesministerium für Bildung und Forschung through contract (05H12GU8), and by the European Commission through contract PITN-GA-2010-264564 (*LHCPhenoNet*).

Note added: While this work was being finalized, a new combination of measurements of the top-quark pair production cross section from the Tevatron appeared [122], which carries a combined experimental uncertainty of 5.4%. This measurements yields $\sigma_{pp\to t\bar{t}} = 7.82 \pm 0.42$ pb for a value of m_t(pole) = 171 GeV for the top-quark pole mass, which is consistent with the NNLO cross section prediction $\sigma_{pp\to t\bar{t}} = 7.17\ ^{+0.22}_{-0.31}\ ^{+0.16}_{-0.16}$ pb based on the ABM12 PDFs at NNLO within the uncertainties.

A A fast algorithm for involved computations in PDF fits

The accommodation of the different data sets for the PDF fit demands very involved computations of the QCD corrections to the Wilson coefficients. In particular this applies to the calculation of the rapidity distribution of the W- and Z-boson decay products produced in hadronic collisions, which are based on the fully exclusive NNLO codes `DYNNLO` [41] and `FEWZ` [42]. The typical CPU runtime needed to achieve a calculation accuracy of much better than the uncertainty of the present data using the codes [41, 42] amounts to $O(100)$ hours. Therefore an iterative use of the available fully exclusive DY codes in the QCD fit is widely impossible. Instead, these codes are commonly

run in advance for the variety of PDF sets, covering the foreseeable spread in the PDF variation, the results of which are stored grids. Afterwards the cross section values for a given PDF set can be computed in a fast manner using linear grid interpolations. For the first time this approach was implemented in the code `fastNLO` [123] for the NLO corrections to the jet productions cross sections. A similar approach is also used in the code `AppleGrid` [124] which provides a tool for generating the cross section grids of different processes, including the DY process. Since `fastNLO` and `AppleGrid` are tools of general purpose, the PDF basis used to generate those grids need to be sufficiently wide to cover the differences between the existing PDF sets. Meanwhile the possible variations of the PDFs in a particular fit are not very large, i.e. if a new fit is aimed to accommodate a new data set being in sufficient agreement with those used in earlier versions of the fit, one may expect variations of the PDFs being comparable to their uncertainties. In this case the PDF basis used to generate the grids for the cross section can be reliably selected as a PDF-bunch, which encodes the uncertainties in a given PDF set. For the PDF uncertainties estimated with the Hessian method this bunch is provided by the PDF set members corresponding to the 1σ variation in the fitted parameters. This allows to minimize the size of the pre-calculated cross section grids and reduces the CPU time necessary to generate these grids correspondingly. Moreover, the structure of the calculation algorithm in using these grids for the PDF fit turns out to be simple. In this appendix we describe, how this approach is implemented in the present analysis.

Firstly, we remind the basics of the PDF uncertainty handling, see Ref. [6] for details. Let $\vec{q}(P_i)$ be the vector of parton distributions encoding the gluon and quark species. It depends on the PDF parameters P_i with the index $i \in [1, N_p]$ and N_p the number of parameters. P_i^0 denote the parameter values obtained in the PDF fit and ΔP_i are their standard deviations. In general the errors in the parameters are correlated, which is expressed by a non-diagonal covariance matrix C_{ij}. However, it is diagonal in the basis of the covariance matrix' eigenvectors which makes this basis particular convenient for the computation of the PDF error. The vector of the parameters P_i transformed into the eigenvector basis reads

$$\tilde{P}_i = \sum_{k=1}^{N_p} \left(\sqrt{C} \right)^{-1}_{ik} P_k \,, \tag{A.1}$$

where

$$\sqrt{C}_{ij} = \sum_{k=1}^{N_p} A_{ik} \sqrt{D}_{kj} \,. \tag{A.2}$$

Here A_{ik} denotes the matrix with the columns given by the orthonormal eigenvectors of C_{ij}, $\sqrt{D}_{kj} = \delta_{jk} \sqrt{e_k}$, e_k are the eigenvalues of C_{ij}, and δ_{jk} is the Kronecker symbol. The PDF uncertainties are commonly presented as the shifts in $\vec{q}$ due to variation of the parameters $\tilde{P}_i$ by their standard deviation. Since the latter are equal to one the shifts are given by

$$\frac{d\vec{q}}{d\tilde{P}_i} = \sum_{k=1}^{N_p} \frac{d\vec{q}}{dP_k} \left(\sqrt{C} \right)_{ik} \,. \tag{A.3}$$

Moreover, the parameters $\tilde{P}_i$ are uncorrelated. Therefore the shifts in Eq. (A.3) can be combined in quadrature to obtain the total PDF uncertainty. In a similar way the uncertainty in a theoretical prediction $t(\vec{q})$ due to the PDFs can be obtained assuming its linear dependence on the PDFs as a combination of the variations

$$\Delta t^{(k)} = t\left[\vec{q}(P_k^0) + \frac{d\vec{q}}{d\tilde{P}_k} \right] - t\left[\vec{q}(P_k^0) \right] \tag{A.4}$$

in quadrature.

Now we show how new data on the hadronic hard-scattering process can be consistently accommodated into the PDF fit avoiding involved cross section computations. Let $P_i^{\rm fit}$ the current values of the PDF parameters in the fit with the new data set included and $\delta P_i = P_i^{\rm fit} - P_i^0$, where P_i^0 stands for the PDF parameter values obtained in the earlier version of the fit performed without the new data-set. The current PDF value can be expressed in terms of δP_i and the PDF variation in the eigenvector basis as follows

$$\vec{q}^{\rm fit} = \vec{q}(P_i^0) + \frac{d\vec{q}}{d\tilde{P}_i}\delta\tilde{P}_i \ , \tag{A.5}$$

where

$$\delta\tilde{P}_i = \sum_{k=1}^{N_p} \left(\sqrt{C}\right)^{-1}_{ik} \delta P_i \ . \tag{A.6}$$

A shift in the hard-scattering cross section corresponding to the variation of the i-th PDF parameter in the fit reads

$$\delta t^{(k)} = t\left[\vec{q}(P_k^0) + \frac{d\vec{q}}{d\tilde{P}_k}\delta\tilde{P}_k\right] - t\left[\vec{q}(P_k^0)\right] \approx \Delta t^{(k)} \sum_{l=1}^{N_p} \left(\sqrt{C}\right)^{-1}_{il} \delta P_i \tag{A.7}$$

and the total change in t is the sum of terms in Eq. (A.7) over all parameters being fitted. The approximation Eq. (A.7) allows fast calculations of the cross section for the new data added to the PDF fit since the values of $\sigma\left[\vec{q}(P_i^0)\right]$ and $\Delta\sigma_i$ can be prepared in advance. This approach is justified if the variation of the parameters in the new fit is localized within their uncertainties obtained in the previous fit or in case of sufficient linearity of the PDFs with respect to the fitted parameters and the cross sections depending on the PDFs. Furthermore, if the algorithm does not seem to guarantee sufficient accuracy, it can be applied iteratively, with the update of the $\sigma\left[\vec{q}(P_i^0)\right]$ and Δt_i values at each iteration.

References

[1] Particle Data Group, J. Beringer *et al.*, Phys.Rev. **D86**, 010001 (2012).

[2] S. Moch, J. Vermaseren, and A. Vogt, Nucl.Phys. **B688**, 101 (2004), hep-ph/0403192.

[3] A. Vogt, S. Moch, and J. Vermaseren, Nucl.Phys. **B691**, 129 (2004), hep-ph/0404111.

[4] S. Alekhin, Phys.Lett. **B519**, 57 (2001), hep-ph/0107197.

[5] S. Alekhin, J. Blümlein, S. Klein, and S. Moch, Phys.Rev. **D81**, 014032 (2010), arXiv:0908.2766.

[6] S. Alekhin, J. Blümlein, and S. Moch, Phys.Rev. **D86**, 054009 (2012), arXiv:1202.2281.

[7] S. Alekhin *et al.*, Phys.Lett. **B697**, 127 (2011), arXiv:1011.6259.

[8] S. Alekhin, J. Blümlein, and S. Moch, PoS **LL2012**, 016 (2012), arXiv:1302.1516.

[9] S. Alekhin, J. Blümlein, and S. Moch, (2013), arXiv:1303.1073.

[10] S. Alekhin, J. Blümlein, and S. Moch, (2013), arXiv:1307.1219.

[11] S. Alekhin, J. Blümlein, and S. Moch, (2013), arXiv:1308.5166.

[12] H1 Collaboration, ZEUS Collaboration, H. Abramowicz *et al.*, Eur.Phys.J. **C73**, 2311 (2013), arXiv:1211.1182.

[13] H1 and ZEUS Collaboration, F. Aaron *et al.*, JHEP **1001**, 109 (2010), arXiv:0911.0884.

[14] ATLAS Collaboration, G. Aad *et al.*, Phys.Rev. **D85**, 072004 (2012), arXiv:1109.5141.

[15] LHCb Collaboration, R. Aaij *et al.*, JHEP **1206**, 058 (2012), arXiv:1204.1620.

[16] CMS Collaboration, S. Chatrchyan *et al.*, Phys.Rev.Lett. **109**, 111806 (2012), arXiv:1206.2598.

[17] LHCb collaboration, R. Aaij *et al.*, JHEP **1302**, 106 (2013), arXiv:1212.4620.

[18] ATLAS Collaboration, (2012), ATLAS-CONF-2012-024.

[19] CMS Collaboration, S. Chatrchyan *et al.*, JHEP **1211**, 067 (2012), arXiv:1208.2671.

[20] ATLAS Collaboration, (2012), ATLAS-CONF-2012-149.

[21] CMS Collaboration, (2012), CMS-PAS-TOP-12-003.

[22] CMS Collaboration, (2012), CMS-PAS-TOP-12-006.

[23] The Tevatron electroweak working group, (2012), D0 Note 6363.

[24] E. Laenen, S. Riemersma, J. Smith, and W. van Neerven, Nucl.Phys. **B392**, 229 (1993).

[25] I. Bierenbaum, J. Blümlein, and S. Klein, Phys.Lett. **B672**, 401 (2009), arXiv:0901.0669.

[26] H. Kawamura, N. Lo Presti, S. Moch, and A. Vogt, Nucl.Phys. **B864**, 399 (2012), arXiv:1205.5727.

[27] N. Lo Presti, H. Kawamura, S. Moch, and A. Vogt, PoS **DIS2010**, 163 (2010), arXiv:1008.0951.

[28] S. Catani, M. Ciafaloni, and F. Hautmann, Nucl.Phys. **B366**, 135 (1991).

[29] I. Bierenbaum, J. Blümlein, and S. Klein, Nucl.Phys. **B780**, 40 (2007), hep-ph/0703285.

[30] I. Bierenbaum, J. Blümlein, S. Klein, and C. Schneider, Nucl.Phys. **B803**, 1 (2008), arXiv:0803.0273.

[31] I. Bierenbaum, J. Blümlein, and S. Klein, Nucl.Phys. **B820**, 417 (2009), arXiv:0904.3563.

[32] J. Ablinger *et al.*, Nucl.Phys. **B844**, 26 (2011), arXiv:1008.3347.

[33] S. Alekhin *et al.*, Phys.Lett. **B720**, 172 (2013), arXiv:1212.2355.

[34] S. Alekhin and S. Moch, (2011), arXiv:1107.0469.

[35] M. Klein and T. Riemann, Z.Phys. **C24**, 151 (1984).

[36] A. Arbuzov *et al.*, Comput.Phys.Commun. **94**, 128 (1996), hep-ph/9511434.

[37] J. Vermaseren, A. Vogt, and S. Moch, Nucl.Phys. **B724**, 3 (2005), hep-ph/0504242.

[38] http://www-zeuthen.desy.de/~alekhin/OPENQCDRAD.

[39] M. Glück, E. Reya, and M. Stratmann, Nucl.Phys. **B422**, 37 (1994).

[40] S. Alekhin, J. Blümlein, and S. Moch, in preparation.

[41] S. Catani *et al.*, Phys.Rev.Lett. **103**, 082001 (2009), arXiv:0903.2120.

[42] Y. Li and F. Petriello, Phys.Rev. **D86**, 094034 (2012), arXiv:1208.5967.

[43] P. Bärnreuther, M. Czakon, and A. Mitov, Phys.Rev.Lett. **109**, 132001 (2012), arXiv:1204.5201.

[44] M. Czakon and A. Mitov, JHEP **1212**, 054 (2012), arXiv:1207.0236.

[45] M. Czakon and A. Mitov, JHEP **1301**, 080 (2013), arXiv:1210.6832.

[46] M. Czakon, P. Fiedler, and A. Mitov, Phys.Rev.Lett. **110**, 252004 (2013), arXiv:1303.6254.

[47] U. Langenfeld, S. Moch, and P. Uwer, Phys.Rev. **D80**, 054009 (2009), arXiv:0906.5273.

[48] M. Aliev *et al.*, Comput.Phys.Commun. **182**, 1034 (2011), arXiv:1007.1327.

[49] S. Alekhin, A. Djouadi, and S. Moch, Phys.Lett. **B716**, 214 (2012), arXiv:1207.0980.

[50] N. Gray, D. J. Broadhurst, W. Grafe, and K. Schilcher, Z.Phys. **C48**, 673 (1990).

[51] K. Chetyrkin and M. Steinhauser, Nucl.Phys. **B573**, 617 (2000), hep-ph/9911434.

[52] K. Melnikov and T. v. Ritbergen, Phys.Lett. **B482**, 99 (2000), hep-ph/9912391.

[53] CMS Collaboration, (2012), CMS-PAS-TOP-12-022.

[54] M. Whalley, D. Bourilkov, and R. Group, (2005), hep-ph/0508110.

[55] LHAPDF, http://hepforge.cedar.ac.uk/lhapdf/.

[56] M. Czakon, M. L. Mangano, A. Mitov, and J. Rojo, JHEP **1307**, 167 (2013), arXiv:1303.7215.

[57] P. Jimenez-Delgado and E. Reya, Phys.Rev. **D79**, 074023 (2009), arXiv:0810.4274.

[58] A. Martin, W. Stirling, R. Thorne, and G. Watt, Eur.Phys.J. **C63**, 189 (2009), arXiv:0901.0002.

[59] R. D. Ball *et al.*, Nucl.Phys. **B867**, 244 (2013), arXiv:1207.1303.

[60] J. Gao *et al.*, (2013), arXiv:1302.6246.

[61] A. Gehrmann-De Ridder, T. Gehrmann, E. Glover, and J. Pires, Phys.Rev.Lett. **110**, 162003 (2013), arXiv:1301.7310.

[62] M. C. Kumar and S. Moch, (2013), arXiv:1309.5311.

[63] H1 Collaboration, C. Adloff *et al.*, Eur.Phys.J. **C21**, 33 (2001), hep-ex/0012053.

[64] NuTeV Collaboration, M. Goncharov *et al.*, Phys.Rev. **D64**, 112006 (2001), hep-ex/0102049.

[65] M. Glück, S. Kretzer, and E. Reya, Phys.Lett. **B380**, 171 (1996), hep-ph/9603304.

[66] T. Gottschalk, Phys.Rev. **D23**, 56 (1981).

[67] NOMAD Collaboration, O. Samoylov *et al.*, (2013), arXiv:1308.4750.

[68] J. Blümlein, S. Riemersma, W. van Neerven, and A. Vogt, Nucl.Phys.Proc.Suppl. **51C**, 97 (1996), hep-ph/9609217.

[69] J. Blümlein, H. Böttcher, and A. Guffanti, Nucl.Phys. **B774**, 182 (2007), hep-ph/0607200.

[70] J. Blümlein and H. Böttcher, (2012), arXiv:1207.3170.

[71] M. Glück, E. Reya, and C. Schuck, Nucl.Phys. **B754**, 178 (2006), hep-ph/0604116.

[72] BCDMS Collaboration, A. Benvenuti *et al.*, Phys.Lett. **B223**, 485 (1989).

[73] BCDMS Collaboration, A. Benvenuti *et al.*, Phys.Lett. **B237**, 592 (1990).

[74] New Muon Collaboration, M. Arneodo *et al.*, Phys.Lett. **B309**, 222 (1993).

[75] New Muon Collaboration, M. Arneodo *et al.*, Nucl.Phys. **B483**, 3 (1997), hep-ph/9610231.

[76] L. Whitlow *et al.*, Phys.Lett. **B250**, 193 (1990).

[77] A. Bodek *et al.*, Phys.Rev. **D20**, 1471 (1979).

[78] W. Atwood *et al.*, Phys.Lett. **B64**, 479 (1976).

[79] M. Mestayer *et al.*, Phys.Rev. **D27**, 285 (1983).

[80] J. Gomez *et al.*, Phys.Rev. **D49**, 4348 (1994).

[81] S. Dasu *et al.*, Phys.Rev. **D49**, 5641 (1994).

[82] FNAL E866/NuSea Collaboration, R. Towell *et al.*, Phys.Rev. **D64**, 052002 (2001), hep-ex/0103030.

[83] G. Moreno *et al.*, Phys.Rev. **D43**, 2815 (1991).

[84] M. Glück, P. Jimenez-Delgado, and E. Reya, Eur.Phys.J. **C53**, 355 (2008), arXiv:0709.0614.

[85] S. Alekhin, J. Blümlein, and S. Moch, (2011), arXiv:1105.5349.

[86] R. D. Ball *et al.*, JHEP **1304**, 125 (2013), arXiv:1211.5142.

[87] S. Forte and G. Watt, (2013), arXiv:1301.6754.

[88] R. D. Ball *et al.*, Phys.Lett. **B707**, 66 (2012), arXiv:1110.2483.

[89] P. Baikov, K. Chetyrkin, J. Kühn, and J. Rittinger, Phys.Rev.Lett. **108**, 222003 (2012), arXiv:1201.5804.

[90] R. Thorne, https://indico.desy.de/contributionDisplay.py?sessionId=24&contribId=78&confId=6889.

[91] S. Alekhin, J. Blümlein, and S. Moch, Eur.Phys.J. **C71**, 1723 (2011), arXiv:1101.5261.

[92] B. Malaescu and P. Starovoitov, Eur.Phys.J. **C72**, 2041 (2012), arXiv:1203.5416.

[93] CMS Collaboration, S. Chatrchyan *et al.*, (2013), arXiv:1304.7498.

[94] S. Lionetti *et al.*, Phys.Lett. **B701**, 346 (2011), arXiv:1103.2369.

[95] A. Martin, W. Stirling, R. Thorne, and G. Watt, Eur.Phys.J. **C64**, 653 (2009), arXiv:0905.3531.

[96] P. Jimenez-Delgado and E. Reya, privat communication October 2013 and in preparation.

[97] R. Abbate *et al.*, Phys.Rev. **D86**, 094002 (2012), arXiv:1204.5746.

[98] T. Gehrmann, G. Luisoni, and P. F. Monni, Eur.Phys.J. **C73**, 2265 (2013), arXiv:1210.6945.

[99] G. Dissertori *et al.*, Phys.Rev.Lett. **104**, 072002 (2010), arXiv:0910.4283.

[100] P. Baikov, K. Chetyrkin, and J. H. Kühn, Phys.Rev.Lett. **101**, 012002 (2008), arXiv:0801.1821.

[101] S. Bethke *et al.*, (2011), arXiv:1110.0016.

[102] D. Boito *et al.*, Phys.Rev. **D85**, 093015 (2012), arXiv:1203.3146.

[103] PACS-CS Collaboration, S. Aoki *et al.*, JHEP **0910**, 053 (2009), arXiv:0906.3906.

[104] C. McNeile *et al.*, Phys.Rev. **D82**, 034512 (2010), arXiv:1004.4285.

[105] B. Blossier *et al.*, Phys.Rev.Lett. **108**, 262002 (2012), arXiv:1201.5770.

[106] A. Bazavov *et al.*, Phys.Rev. **D86**, 114031 (2012), arXiv:1205.6155.

[107] E. Shintani *et al.*, Phys.Rev. **D82**, 074505 (2010), arXiv:1002.0371.

[108] S. Bethke, Nucl.Phys.Proc.Suppl. **234**, 229 (2013), arXiv:1210.0325.

[109] J. Blümlein, A. Hasselhuhn, S. Klein, and C. Schneider, Nucl.Phys. **B866**, 196 (2013), arXiv:1205.4184.

[110] J. Ablinger *et al.*, Nucl.Phys. **B864**, 52 (2012), arXiv:1206.2252.

[111] J. Blümlein *et al.*, XXI International Workshop on Deep-Inelastic Scattering and Related Subjects -DIS2013 , Marseilles, France (2013), arXiv:1307.7548.

[112] R. Thorne and W. Tung, (2008), arXiv:0809.0714.

[113] T. Stavreva *et al.*, Phys.Rev. **D85**, 114014 (2012), arXiv:1203.0282.

[114] R. Hamberg, W. van Neerven, and T. Matsuura, Nucl.Phys. **B359**, 343 (1991).

[115] R. V. Harlander and W. B. Kilgore, Phys.Rev.Lett. **88**, 201801 (2002), hep-ph/0201206.

[116] C. Anastasiou and K. Melnikov, Nucl.Phys. **B646**, 220 (2002), hep-ph/0207004.

[117] V. Ravindran, J. Smith, and W. L. van Neerven, Nucl.Phys. **B665**, 325 (2003), hep-ph/0302135.

[118] V. Ravindran, J. Smith, and W. van Neerven, Nucl.Phys. **B704**, 332 (2005), hep-ph/0408315.

[119] LHC Higgs Cross Section Working Group, S. Heinemeyer *et al.*, (2013), arXiv:1307.1347.

[120] S. Moch and A. Vogt, Phys.Lett. **B631**, 48 (2005), hep-ph/0508265.

[121] LHC Higgs Cross Section Working Group, S. Dittmaier *et al.*, (2012), arXiv:1201.3084.

[122] CDF & D0 Collaboration, T. A. Aaltonen *et al.*, (2013), arXiv:1309.7570.

[123] fastNLO Collaboration, M. Wobisch *et al.*, (2011), arXiv:1109.1310.

[124] T. Carli *et al.*, Eur.Phys.J. **C66**, 503 (2010), arXiv:0911.2985.